MMSE Design of RIS-Aided Communications with Spatially-Correlated Channels and Electromagnetic Interference

MMSE Design of RIS-Aided Communications with Spatially-Correlated Channels and Electromagnetic Interference

Wen-Xuan Long, *Member, IEEE*, Marco Moretti, *Member, IEEE*, Andrea Abrardo, *Senior Member, IEEE*, Luca Sanguinetti, *Senior Member, IEEE* and Rui Chen, *Member, IEEE*

***Abstract*—Consider a communication system in which a single-antenna user equipment exchanges information with a multi-antenna base station via a reconfigurable intelligent surface (RIS) in the presence of spatially correlated channels and electromagnetic interference (EMI). To exploit the attractive advantages of RIS technology, accurate configuration of its reflecting elements is crucial. In this paper, we use statistical knowledge of channels and EMI to optimize the RIS elements for *i*) accurate channel estimation and *ii*) reliable data transmission. In both cases, our goal is to determine the RIS coefficients that minimize the mean square error, resulting in the formulation of two non-convex problems that share the same structure. To solve these two problems, we present an alternating optimization approach that reliably converges to a locally optimal solution. The incorporation of the diagonally scaled steepest descent algorithm, derived from Newton's method, ensures fast convergence with manageable complexity. Numerical results demonstrate the effectiveness of the proposed method under various propagation conditions. Notably, it shows significant advantages over existing alternatives that depend on a suboptimal configuration of the RIS and are derived on the basis of different criteria.**

***Index Terms*—Reconfigurable intelligent surface (RIS), electromagnetic interference (EMI), channel estimation, spectral efficiency, minimum mean square error (MMSE), spatially correlated channels.**

I. Introduction

Reconfigurable intelligent surfaces (RIS) have received remarkable interest in the context of next-generation wireless systems [1]–[4]. A RIS comprises a planar array of M reflective elements positioned at sub-wavelength intervals. Each element's impedance can be adjusted to introduce a controllable phase-shift to the incoming wave before reflecting it. By optimizing the phase-shift pattern throughout the RIS, it becomes possible to control the reflected wavefront and shape it into a directed beam aimed at the intended receiver [4]. In a communication system in which a single-antenna user equipment (UE) exchanges information with a multi-antenna base station (BS) via a RIS, accurate estimation of the cascaded channel (from the UE to RIS and from the RIS to the BS) is crucial to properly design the phase-shifts and harness the attractive advantages of the RIS technology. Nevertheless, this is a complicated task, primarily due to passive nature of the RIS and the challenges posed by high-dimensional channels [5], [6]. The existence of electromagnetic interference (EMI) [7]–[11], which can occur naturally in any environment [12], [13], further complicates the task. The aim of this paper is to design the elements of the RIS with the primary goal of initially achieving a precise estimate of the cascaded channel and subsequently enhancing the spectral efficiency (SE) of the system. In contrast to most of previous studies, we consider the existence of EMI.

A. Relevant literature

The quality of channel state information (CSI) plays a critical role in determining the performance of RIS-based communications. As a passive device, a RIS cannot estimate the channel locally or actively transmit pilot signals. Therefore, channel estimation must be performed at the BS or UE. In single-user systems, the least-square (LS) estimator [14], [15], the reduced-subspace LS (RS-LS) estimator [6], the bilinear generalized approximate message passing algorithm [16] and the bilinear adaptive vector approximate message passing algorithm [17] can be employed to accurately estimate the cascaded channel. In multi-user scenarios, the PARAllel FACtor-based channel estimation framework is introduced in [18] to efficiently estimate the cascaded channels; while in [19], exploiting the linear correlation among multi-user cascaded channels, the estimation of the angle information of the BS-RIS channel is combined with the LS estimator used to estimate the channel gains, significantly reducing the pilot overhead. Besides, the always-ON channel estimation protocol is proposed in [20], which greatly reduces the required pilot overhead by exploiting the common-link structure of multi-user cascaded channels. Moreover, a two-step multi-user joint channel estimation method based on compressed sensing is

W.-X. Long is with the Dipartimento di Ingegneria dell'Informazione, University of Pisa, Pisa, Italy, and also with the State Key Laboratory of Integrated Service Networks (ISN), Xidian University, Shaanxi 710071, China (e-mail: wen-xuan.long@ing.unipi.it).

M. Moretti and L. Sanguinetti are with the Dipartimento di Ingegneria dell'Informazione, University of Pisa, Pisa, Italy, and also with CNIT (National Interuniversity Consortium for Telecommunications) (email: marco.moretti@unipi.it, luca.sanguinetti@unipi.it).

A. Abrardo is with the Department of Information Engineering and Mathematical Sciences of the University of Siena, and also with CNIT (email: abrardo@unisi.it).

R. Chen is with the State Key Laboratory of Integrated Service Networks (ISN), Xidian University, Shaanxi 710071, China (e-mail: rchen@xidian.edu.cn).

L. Sanguinetti, M. Moretti and W.-X. Long are partially supported by the Italian Ministry of Education and Research (MUR) in the framework of the FoReLab project (Departments of Excellence) and by the Project GARDEN, funded by EU in NextGenerationEU plan through the Italian "Bando Prin 2022 - D.D. 1409 del 14-09-2022". A. Abrardo is supported by the European community within the 6G SHINE project (6G SHort range extreme communication IN Entities). R. Chen is partially supported by the National Natural Science Foundation of China under Grant 62271376.

proposed in [21] to acquire CSIs of multiple users simultaneously, taking advantage of the sparsity of cascaded channels.

After accurate channel estimation, appropriate RIS phase configuration is also crucial for RIS-aided data transmission. Under the assumption of known CSI, in RIS-aided single-user systems, [22] applies the branch-and-bound method to design the optimal RIS configuration with the criterion of minimizing the transmit power; while [23] proposes the deep deterministic policy gradient algorithm to obtain the optimal RIS phase shifts to maximize the downlink received SNR. In [24], to maximize the ergodic SE, the optimal RIS phase shifts are derived using the semidefinite relaxation algorithm under the premise of shaping the transmitted beamforming with the principal eigenvector of the channel. Similarly, for multi-user systems, the genetic algorithm [25] and the gradient projection method [26] are applied to design the optimal RIS phase shifts for maximizing the minimum signal-to-interference-plus-noise ratio (SINR), thus ensuring balanced performance among different users. In [27], the transmit beamforming vector and RIS phase shifts are alternately optimized using the Lagrangian multiplier method and the distributed alternating direction method of multipliers, respectively, to maximize the sum rate.

Besides, as a passive device, the RIS does not amplify signals, but relies on directional reflection. Therefore, to ensure a satisfactory signal-to-noise ratio (SNR) at the receiver, RIS is required to be equipped with a significant surface area for wireless communications. As the size of the RIS increases, it becomes more susceptible to EMI, which may originate from various natural causes, such as atmospheric noise [12], or result from intentional or unintentional human activities, such as signals serving other users [28] or radiation from power lines [12]. In [7], the authors show that the EMI power reflected by the RIS may severely affect the system performance since it grows proportionally to the RIS size. However, to the best of our knowledge, the existing studies on RIS-aided communications typically ignore the EMI, and only a few papers have considered the impact of EMI. In [7], the SINR for RIS-aided communications in the presence of EMI is derived, indicating that the SINR only increases linearly with the RIS size, rather than the conventional squared growth without interference. Based on this SINR, [8] quantitatively analyze the block error rate, capacity and system goodput of RIS-aided communications with EMI. Additionally, [9] point out that the EMI may pose a potential threat to the physical layer security of RIS-aided communications. Hence, the EMI is an unavoidable factor that needs to be considered in the design of RIS-aided communications. In our recent paper [10], the cascaded channel of an RIS-aided system under constant EMI is accurately estimated using a conservative RS-LS estimator. Under the same assumption of constant EMI, [11] present the first EMI cancellation method applicable to the RIS-aided data transmission.

B. Contribution

As discussed above, reliable RIS-based data transmission depends on accurate CSI. However, existing research on channel estimation and data transmission in RIS-aided systems is generally considered as two separate components, each designed based on different criteria. To the best of our knowledge, there are few papers that jointly consider the channel estimation and data transmission in RIS-aided systems and optimize the overall configuration of RIS based on a unified criteria. Among them, there are [29] and [30], in which the optimization of the RIS for data transmission is performed based on the statistical knowledge of the node location. The validity of such approaches is therefore limited to cases where the channel is closely related to the node positions, namely in scenarios where there is a strong line-of-sight (LoS) component in both the BS-RIS and RIS-UE links. To overcome the above issues, in this paper we aim to design both the channel estimation and data transmission for RIS-aided communications using a unified criterion. Besides considering more general channel models, we also take into account the presence of EMI, which cannot be generally neglected due to the nature of RIS. In this respect, existing literature assumes that the interference experienced by RIS-based communications is approximately constant throughout the entire period, while how to efficiently configure the RIS phase shifts in the presence of random interference for accurate channel estimation and data transmission remains an open issue. To address these issues, this paper aims to propose a joint design framework for RIS-aided communications in the presence of random interference. In summary, our main contributions are as follows:

- We first derive the linear minimum mean square error (LMMSE) estimator for the cascaded channel and then employ this estimate to formulate the LMMSE combiner at the BS with the aim of improving the SE. In both instances, the efficacy of the estimator and combiner hinges on the phase-shift coefficients of the RIS. To optimize overall performance, we investigate a scheme designed to determine the RIS elements, with the goal of minimizing the MSE separately for both channel estimation and data transmission.
- Since both instances involve solving a non-convex problem to compute the optimal RIS configuration, we first propose an ad-hoc factorization of the MMSE and then we provide an iterative algorithm, which ensures convergence to a locally optimal solution.
- The optimization algorithms, employing the principle of *alternating optimization* (AO), leverage the knowledge of the second-order statistics of channels and EMI to implement a projected gradient scheme based on a novel variant of Newton's method, which balances convergence speed with low computational load.
- Numerical results validate the method's efficacy across various propagation conditions, highlighting its substantial advantages over existing alternatives relying on sub-optimal RIS configurations.

C. Paper Outline and Notation

The remainder of this paper is organized as follows. In Section II, we introduce the model adopted for the system, propagation channels and EMI. In Section III, the channel

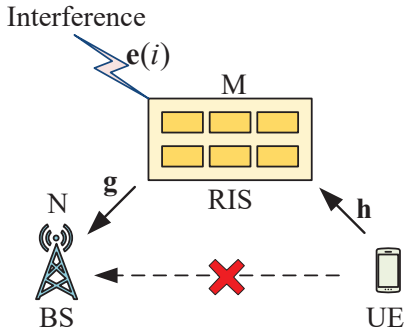

Fig. 1: RIS-aided communication system.

estimation problem is addressed by means of the LMMSE criterion, followed by the SE computation using the LMMSE combining scheme, which minimizes the MSE between the data signal and the received signal after combining. In Section IV, we provide an iterative algorithm with provable convergence that allows to optimize the RIS according to the MSE criteria adopted in the channel estimation and data transmission phases. Numerical results are given in Section V while conclusions are drawn in Section VI.

Matrices are denoted by bold uppercase letters (i.e., $\mathbf{X}$), vectors are represented by bold lowercase letters (i.e., $\mathbf{x}$), and scalars are denoted by normal font (i.e., x). $(\cdot)^{\mathrm{T}}$, $(\cdot)^{\mathrm{H}}$ and $(\cdot)^{-1}$ stand for the transpose, Hermitian transpose and inverse of the matrices. The symbol $\otimes$ represents the Kronecker matrix product, while $\odot$ represents the Hadamard product. The notation $\mathbf{x} = \mathrm{vec}(\mathbf{X})$ defines the linear transformation that converts an $P \times Q$-dimensional $\mathbf{X}$ into a column vector $\mathbf{x}$ with size $PQ \times 1$ by stacking the columns of $\mathbf{X}$ on top of each other, $||\mathbf{x}||$ signifies the Euclidean norm of the vector $\mathbf{x}$, and $\mathrm{tr}\{\mathbf{X}\}$ indicates the trace of the square matrix $\mathbf{X}$. The notation $\mathbb{E}\{\cdot\}$ represents the statistical expectation, $\mathrm{mod}\,(\cdot,\cdot)$ denotes the modulus operation and $\lfloor\cdot\rfloor$ truncates the argument.

II. System Model

We consider the RIS-aided communication[1] from a single-antenna UE to an N-element BS, as shown in Fig. 1. The RIS is equipped with M passive reconfigurable elements, forming a uniform planar array (UPA) with M_H rows and M_V columns, where $M = M_H M_V$. The horizontal and vertical element spacing is set to d_M, and the elements are labeled row-by-row as $m \in [1, M]$. Then, the location of the m-th element relative to the origin can be expressed as $\mathbf{u}_m = [0, \mathrm{mod}\,(m-1, M_V)d_M, \lfloor (m-1)/M_V \rfloor d_M]^{\mathrm{T}}$ [31]. When a plane-wave impinges on the RIS from the azimuth angle φ and elevation angle ϑ, the array response vector can be written as [32]

$$\mathbf{a}(\varphi,\vartheta) = \left[e^{\jmath \mathbf{k}^{\mathrm{T}}(\varphi,\vartheta)\mathbf{u}_1}, \ldots, e^{\jmath \mathbf{k}^{\mathrm{T}}(\varphi,\vartheta)\mathbf{u}_M}\right]^{\mathrm{T}}, \tag{1}$$

where

$$\mathbf{k}(\varphi,\vartheta) = \frac{2\pi}{\lambda}[\cos\vartheta\cos\varphi, \cos\vartheta\sin\varphi, \sin\vartheta]^{\mathrm{T}} \tag{2}$$

is the wave vector and λ is the wavelength. The BS antennas are also deployed as a UPA [32] with N_H rows and N_V columns, so that $N = N_H N_V$. The horizontal and vertical antenna spacing is set to d_N. The array response vector at the BS has the same form as (1) but uses the antenna spacing d_N of the BS [32].

We consider a block-fading model where each channel takes one realization in a coherence block of τ_c channel uses and independent realizations across blocks. The channel from the UE to the RIS is called $\mathbf{h}$ and modelled as the correlated Rayleigh fading channel[2] $\mathbf{h} \sim \mathcal{N}_{\mathbb{C}}(\mathbf{0}_M, \mathbf{R}_h)$ [31], [32], with $\mathbf{R}_h \in \mathbb{C}^{M\times M}$ being the spatial correlation matrix:

$$\mathbf{R}_h = \beta_h \int_{\vartheta_L}^{\vartheta_U}\int_{\varphi_L}^{\varphi_U} f_h(\varphi,\vartheta)\mathbf{a}(\varphi,\vartheta)\mathbf{a}^{\mathrm{H}}(\varphi,\vartheta)d\vartheta d\varphi, \tag{3}$$

where β_h is the channel gain, and $f_h(\varphi,\vartheta)$ is the normalized spatial scattering function with $\iint f_h(\varphi,\vartheta)d\vartheta d\varphi = 1$.

The narrowband channel from the m-th RIS element to the n-th BS element is indicated as $g_{m,n}$. We call $\mathbf{g}_n = [g_{n,1}, g_{n,2}, \ldots, g_{n,M}]^{\mathrm{T}} \in \mathbb{C}^M$ the channel vector from the RIS to the n-th BS element, while $\mathbf{g}'_m = [g_{1,m}, g_{2,m}, \cdots, g_{N,m}]^{\mathrm{T}} \in \mathbb{C}^N$ denotes the channel vector from the m-th RIS element to the BS array. Using the Kronecker model [5], [33], we have that

$$\mathbf{g}_n \sim \mathcal{N}_{\mathbb{C}}(\mathbf{0}_M, [\mathbf{R}_{g'_m}]_{n,n}\mathbf{R}_{g_n}) \tag{4}$$

$$\mathbf{g}'_m \sim \mathcal{N}_{\mathbb{C}}(\mathbf{0}_N, [\mathbf{R}_{g_n}]_{m,m}\mathbf{R}_{g'_m}) \tag{5}$$

where $[\mathbf{R}_{g'_m}]_{n,n}\mathbf{R}_{g_n}$ and $[\mathbf{R}_{g_n}]_{m,m}\mathbf{R}_{g'_m}$ are the spatial correlation matrices of $\mathbf{g}_n$ and $\mathbf{g}'_m$, respectively. Both $\mathbf{R}_{g_n}$ and $\mathbf{R}_{g'_m}$ have the same form as (3) but must be computed using the specific spatial scattering function and channel gain corresponding to $\mathbf{g}_n$ and $\mathbf{g}'_m$.

We assume the channels $\mathbf{g}_n$ (and thus $\mathbf{g}'_m$) and $\mathbf{h}$ are independent of each other. The cascaded channel between the UE and the n-th element of the BS is given by the M-dimensional vector

$$\mathbf{x}_n = \mathbf{g}_n \odot \mathbf{h}. \tag{6}$$

A common practice in existing RIS-aided communications is to only consider the signals generated by the system, and thereby neglecting the EMI or "noise" (or "pollution") that is inevitably present in any environment. The EMI may arise from a variety of natural, intentional or non-intentional causes, for example, man-made devices and natural background radiation. In this paper, we call $\mathbf{e}(i) \in \mathbb{C}^M$ the vector collecting the EMI during the i-th channel use, which accounts for any uncontrollable factor (e.g., of electromagnetic or hardware nature) disturbing the incoming signals at the RIS. We model it as $\mathbf{e}(i) \sim \mathcal{N}_{\mathbb{C}}(\mathbf{0}_M, \sigma_e^2\mathbf{R}_e)$ and assume that it takes independent realizations across channel uses, i.e., $\mathbb{E}\{\mathbf{e}(i)\mathbf{e}(i')^{\mathrm{H}}\} = 0$ for $i \neq i'$. The normalized spatial correlation matrix $\mathbf{R}_e \in \mathbb{C}^{M\times M}$ has the same form of (3),

[1]The RIS serves a specific UE with the obstructed direct path to the BS, while signals from other UEs captured by the RIS can be considered EMI.

[2]Although the proposed MMSE solution is derived using the correlated Rayleigh fading model, it can be extended to the Rician and LoS channel models by utilizing the appropriate models.

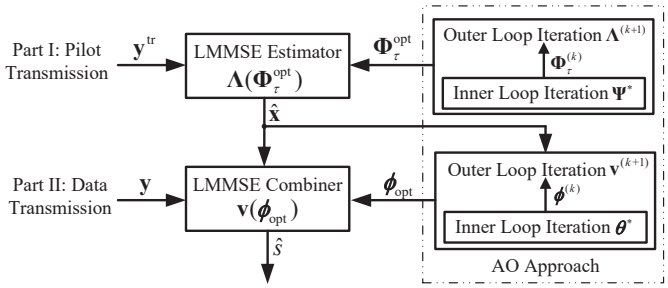

Fig. 2: Block diagram of the receiver based on the minimum MSE criterion in the RIS-aided communication. The communication is divided in two parts: (I) channel estimation, and (II) data transmission.

i.e.,

$$\mathbf{R}_e = \int_{\vartheta_L}^{\vartheta_U}\int_{\varphi_L}^{\varphi_U} f_e(\varphi,\vartheta)\mathbf{a}(\varphi,\vartheta)\mathbf{a}^{\mathrm{H}}(\varphi,\vartheta)d\vartheta d\varphi, \tag{7}$$

but with a different spatial scattering function $f_e(\varphi,\vartheta)$.

III. System Operation

We assume that the system operates according to a communication protocol wherein the data transmission phase is preceded by a training phase for channel estimation, as shown in Fig. 2, where the τ_c available channel uses are employed for: τ for training phase and $\tau_c - \tau$ for uplink payload transmission. Both the training phase and the uplink data transmission phase are designed based on the LMMSE criterion. As the RIS is devised to aid the communication with UEs that have bad or absent direct links, we neglect the direct link from the UE to the BS and focus on the design of RIS phase-shifts aimed at enhancing the performance of the cascaded channel.

A. Pilot Transmission and Linear MMSE Estimation

We assume that the training sequence of length τ is composed by all ones and denote $\boldsymbol{\phi}(i) \in \mathbb{C}^M$ the vector collecting the controllable phase-shifts $\{\phi_m(i) \in [0,2\pi); m = 1,\ldots,M\}$[3] introduced by the RIS during the i-th channel use. The training signals at the RIS can be written as

$$\mathbf{y}_{\mathrm{RIS}}^{\mathrm{tr}}(i) = \sqrt{\rho^{\mathrm{tr}}}\mathbf{h} + \mathbf{e}(i), \tag{8}$$

where ρ^{tr} is the power of the training signal, and $\mathbf{e}(i)$ can be regarded as an additive interference to $\mathbf{h}$. After RIS reflection, the training signal $y_n^{\mathrm{tr}}(i)$ received by the n-th BS antenna takes the form:

$$y_n^{\mathrm{tr}}(i) = \sqrt{\rho^{\mathrm{tr}}}\boldsymbol{\phi}(i)^{\mathrm{T}}\mathbf{x}_n + w_n(i) + z_n(i), \tag{9}$$

where

$$w_n(i) = \boldsymbol{\phi}(i)^{\mathrm{T}}\left(\mathbf{g}_n \odot \mathbf{e}(i)\right) \tag{10}$$

is the EMI reflected from the RIS to the BS, and $z_n(i) \sim \mathcal{N}_{\mathbb{C}}(0,\sigma^2)$ is the additive white Gaussian noise. Notice that the term $w_n(i)$ depend on the RIS configuration. By collecting all the training signals received at the n-th BS antenna during the τ channel uses of the training phase, we obtain $\mathbf{y}_n^{\mathrm{tr}} = [y_n^{\mathrm{tr}}(1),\ldots,y_n^{\mathrm{tr}}(\tau)]^{\mathrm{T}} \in \mathbb{C}^\tau$ given by

$$\mathbf{y}_n^{\mathrm{tr}} = \sqrt{\rho^{\mathrm{tr}}}\mathbf{\Phi}_\tau\mathbf{x}_n + \mathbf{w}_n^{\mathrm{tr}} + \mathbf{z}_n^{\mathrm{tr}}, \tag{11}$$

where

$$\mathbf{\Phi}_\tau = [\boldsymbol{\phi}(1),\boldsymbol{\phi}(2),\cdots,\boldsymbol{\phi}(\tau)]^{\mathrm{T}} \in \mathbb{C}^{\tau\times M}, \tag{12}$$

$\mathbf{w}_n^{\mathrm{tr}} = [w_n(1),\ldots,w_n(\tau)]^{\mathrm{T}}$ and $\mathbf{z}_n^{\mathrm{tr}} = [z_n(1),\ldots,z_n(\tau)]^{\mathrm{T}}$. Accordingly, the vector $\mathbf{y}^{\mathrm{tr}} = [\mathbf{y}_1^{\mathrm{tr}\,\mathrm{T}},\ldots,\mathbf{y}_N^{\mathrm{tr}\,\mathrm{T}}]^{\mathrm{T}} \in \mathbb{C}^{N\tau}$, obtained by collecting the signals received at the BS array during the training phase, takes the form

$$\mathbf{y}^{\mathrm{tr}} = \sqrt{\rho^{\mathrm{tr}}}\mathbf{\Phi}_{N\tau}\mathbf{x} + \mathbf{w}^{\mathrm{tr}} + \mathbf{z}^{\mathrm{tr}} \tag{13}$$

with

$$\mathbf{\Phi}_{N\tau} = \mathbf{I}_N \otimes \mathbf{\Phi}_\tau, \tag{14}$$

and $\mathbf{x} = [\mathbf{x}_1^{\mathrm{T}},\ldots,\mathbf{x}_N^{\mathrm{T}}]^{\mathrm{T}} \in \mathbb{C}^{MN}$, $\mathbf{w}^{\mathrm{tr}} = [\mathbf{w}_1^{\mathrm{tr}\,\mathrm{T}},\ldots,\mathbf{w}_N^{\mathrm{tr}\,\mathrm{T}}]^{\mathrm{T}} \in \mathbb{C}^{N\tau}$ and $\mathbf{z}^{\mathrm{tr}} = [\mathbf{z}_1^{\mathrm{tr}\,\mathrm{T}},\ldots,\mathbf{z}_N^{\mathrm{tr}\,\mathrm{T}}]^{\mathrm{T}} \in \mathbb{C}^{N\tau}$.

Due to the ability to utilize the sensing mode of RIS to obtain the statistical information of channels and EMI [34], we assume that the BS has knowledge of the correlation matrices $\mathbf{R}_x = \mathbb{E}\{\mathbf{x}\mathbf{x}^{\mathrm{H}}\}$ and $\mathbf{R}_w^{\mathrm{tr}} = \frac{1}{\sigma_e^2}\mathbb{E}\{\mathbf{w}^{\mathrm{tr}}(\mathbf{w}^{\mathrm{tr}})^{\mathrm{H}}\}$. These are given by (see Appendix A)

$$\mathbf{R}_x = \mathbf{R}_{g_m'} \otimes (\mathbf{R}_{g_n} \odot \mathbf{R}_h) = \mathbf{R}_{g_m'} \otimes \mathbf{R}_c \tag{15}$$

and

$$\mathbf{R}_w^{\mathrm{tr}} = \mathbf{R}_{g_m'} \otimes \left(\left(\mathbf{\Phi}_\tau\mathbf{R}_q\mathbf{\Phi}_\tau^{\mathrm{H}}\right) \odot \mathbf{I}_\tau\right), \tag{16}$$

where we have defined

$$\mathbf{R}_c = \mathbf{R}_{g_n} \odot \mathbf{R}_h \in \mathbb{C}^{M\times M} \tag{17}$$

and

$$\mathbf{R}_q = \mathbf{R}_{g_n} \odot \mathbf{R}_e \in \mathbb{C}^{M\times M} \tag{18}$$

for subsequent use. If $\tau = 1$, then (16) reduces to

$$\mathbf{R}_w^{\mathrm{tr}} = \mathbf{R}_{g_m'} \otimes \left(\boldsymbol{\phi}^{\mathrm{T}}\mathbf{R}_q\boldsymbol{\phi}^*\right), \tag{19}$$

from which, by applying $(\mathbf{AC})\otimes(\mathbf{BD}) = (\mathbf{A}\otimes\mathbf{B})(\mathbf{C}\otimes\mathbf{D})$ twice, we get

$$\mathbf{R}_w^{\mathrm{tr}} = \mathbf{\Phi}_N\left(\mathbf{R}_{g_m'} \otimes \mathbf{R}_q\right)\mathbf{\Phi}_N^{\mathrm{H}} \tag{20}$$

with

$$\mathbf{\Phi}_N = \mathbf{I}_N \otimes \boldsymbol{\phi}^{\mathrm{T}}. \tag{21}$$

The statistics above are used to compute $\hat{\mathbf{x}}$, the LMMSE estimate of $\mathbf{x}$ based on $\mathbf{y}^{\mathrm{tr}}$.

Lemma 1. *The LMMSE estimate of* $\mathbf{x}$ *based on the observation of* $\mathbf{y}^{\mathrm{tr}}$ *is*

$$\hat{\mathbf{x}} = \frac{1}{\sqrt{\rho^{\mathrm{tr}}}}\mathbf{R}_x\mathbf{\Phi}_{N\tau}^{\mathrm{H}}\left(\mathbf{R}_y^{\mathrm{tr}}\right)^{-1}\mathbf{y}^{\mathrm{tr}}, \tag{22}$$

where $\mathbf{R}_y^{\mathrm{tr}} = \frac{1}{\rho^{\mathrm{tr}}}\mathbb{E}\{\mathbf{y}^{\mathrm{tr}}(\mathbf{y}^{\mathrm{tr}})^{\mathrm{H}}\}$ *is given by*

$$\mathbf{R}_y^{\mathrm{tr}} = \mathbf{\Phi}_{N\tau}\mathbf{R}_x\mathbf{\Phi}_{N\tau}^{\mathrm{H}} + \frac{\sigma_e^2}{\rho^{\mathrm{tr}}}\mathbf{R}_w^{\mathrm{tr}} + \frac{\sigma^2}{\rho^{\mathrm{tr}}}\mathbf{I}_{N\tau}. \tag{23}$$

[3]In practice, due to constraints imposed by the hardware configuration, the phase-shifts of RIS elements are typically discrete. For convenience, we assume here that the RIS phase-shifts are continuously adjustable.

The estimation error $\tilde{\mathbf{x}} = \mathbf{x} - \hat{\mathbf{x}}$ *has correlation matrix*

$$\mathbf{R}_{\tilde{x}} = \mathbb{E}\{\tilde{\mathbf{x}}\tilde{\mathbf{x}}^{\mathrm{H}}\} = \mathbf{R}_x - \mathbf{R}_x\mathbf{Q}^{\mathrm{tr}}(\boldsymbol{\Phi}_\tau)\mathbf{R}_x \tag{24}$$

with

$$\mathbf{Q}^{\mathrm{tr}}(\boldsymbol{\Phi}_\tau) = \boldsymbol{\Phi}_{N\tau}^{\mathrm{H}} \left(\mathbf{R}_y^{\mathrm{tr}}\right)^{-1} \boldsymbol{\Phi}_{N\tau}. \tag{25}$$

Proof: The proof follows from standard arguments and is given in Appendix A for completeness. ∎

From (24), the MSE is given by

$$\mathcal{E}_x(\boldsymbol{\Phi}_\tau) = \mathrm{tr}\left\{\mathbf{R}_{\tilde{x}}\right\} = \mathrm{tr}\left\{\mathbf{R}_x - \mathbf{R}_x\mathbf{Q}^{\mathrm{tr}}(\boldsymbol{\Phi}_\tau)\mathbf{R}_x\right\}, \tag{26}$$

which depends only on $\boldsymbol{\Phi}_\tau$ since the channel statistics are fixed and given.

Remark 1. *A scheme that dispenses from knowledge of statistics is the LS channel estimator [32]. In this case, we have that*

$$\hat{\mathbf{x}} = \frac{1}{\sqrt{\rho^{\mathrm{tr}}}}\mathbf{A}_1\mathbf{y}^{\mathrm{tr}} \tag{27}$$

with $\mathbf{A}_1 = \left(\boldsymbol{\Phi}_{N\tau}^{\mathrm{H}}\boldsymbol{\Phi}_{N\tau}\right)^{-1}\boldsymbol{\Phi}_{N\tau}^{\mathrm{H}}$*, and the MSE takes the form*

$$\mathcal{E}_x'(\boldsymbol{\Phi}_\tau) = \mathrm{tr}\left\{\mathbf{R}_{\mathrm{x}} - 2\Re\mathrm{e}\left(\mathbf{A}_1\boldsymbol{\Phi}_{\mathrm{N}\tau}\mathbf{R}_{\mathrm{x}}\right) + \mathbf{A}_1\mathbf{R}_{\mathrm{y}}^{\mathrm{tr}}\mathbf{A}_1^{\mathrm{H}}\right\}. \tag{28}$$

By using (23) *and* $\mathbf{A}_1\boldsymbol{\Phi}_{N\tau} = \mathbf{I}_{N\tau}$*, we obtain*

$$\mathcal{E}_x'(\boldsymbol{\Phi}_\tau) = \mathrm{tr}\left\{\frac{\sigma_e^2}{\rho^{\mathrm{tr}}}\mathbf{A}_1\mathbf{R}_w^{\mathrm{tr}}\mathbf{A}_1^{\mathrm{H}} + \frac{\sigma^2}{\rho^{\mathrm{tr}}}\left(\boldsymbol{\Phi}_{N\tau}^{\mathrm{H}}\boldsymbol{\Phi}_{N\tau}\right)^{-1}\right\}. \tag{29}$$

Alternatively, one may resort to the RS-LS estimate, which can be obtained by employing the reduced-subspace linear filter [6], i.e.,

$$\hat{\mathbf{x}} = \frac{1}{\sqrt{\rho^{\mathrm{tr}}}}\mathbf{A}_2\mathbf{y}^{\mathrm{tr}} \tag{30}$$

where

$$\mathbf{A}_2 = \mathbf{U}_s\left(\mathbf{U}_s^{\mathrm{H}}\boldsymbol{\Phi}_{N\tau}^{\mathrm{H}}\boldsymbol{\Phi}_{N\tau}\mathbf{U}_s\right)^{-1}\mathbf{U}_s^{\mathrm{H}}\boldsymbol{\Phi}_{N\tau}^{\mathrm{H}}, \tag{31}$$

and $\mathbf{U}_s \in \mathbb{C}^{MN\times r}$ *spans the signal subspace of* $\mathbf{R}_x$ *containing* $\mathbf{x}$*, and* $r = rank\{\mathbf{R}_x\}$*. This estimator has already been applied in the cascaded channel estimation for RIS-aided communications with constant EMI [10]. The MSE is given by*

$$\mathcal{E}_x''(\boldsymbol{\Phi}_\tau) = \mathrm{tr}\left\{\frac{\sigma_e^2}{\rho^{\mathrm{tr}}}\mathbf{A}_2\mathbf{R}_w^{\mathrm{tr}}\mathbf{A}_2^{\mathrm{H}} + \frac{\sigma^2}{\rho^{\mathrm{tr}}}\left(\mathbf{U}_s^{\mathrm{H}}\boldsymbol{\Phi}_{N\tau}^{\mathrm{H}}\boldsymbol{\Phi}_{N\tau}\mathbf{U}_s\right)^{-1}\right\}. \tag{32}$$

When $r < MN$*, the RS-LS estimator offers superior performance compared to the LS estimator due to noise removal from the unused channel dimensions [6].*

Remark 2. *The LMMSE estimator in* (22) *can be applied for any* $\tau \geq 1$*, but better results are achieved for larger values of* τ*. The LS estimator in* (27) *requires* $\tau \geq M$*, which may be large, whereas the RS-LS estimator in* (30) *relaxes the required number of pilots to* $\tau \geq \frac{r}{N}$ *[6].*

B. Uplink Spectral Efficiency and Linear MMSE Combining

Similar to (9), the uplink received signal at the n-th antenna during data transmission is

$$y_n = \sqrt{\rho}\boldsymbol{\phi}^{\mathrm{T}}\mathbf{x}_n s + w_n + z_n, \tag{33}$$

where ρ is the power of the transmitted signal $s \in \mathbb{C}$ and

$$w_n = \boldsymbol{\phi}^{\mathrm{T}}\left(\mathbf{g}_n \odot \mathbf{e}\right) \tag{34}$$

is the reflected EMI. The received vector $\mathbf{y} = [y_1, \ldots, y_N]^{\mathrm{T}} \in \mathbb{C}^N$ at the BS takes the form

$$\mathbf{y} = \sqrt{\rho}\boldsymbol{\Phi}_N\mathbf{x}s + \mathbf{w} + \mathbf{z}, \tag{35}$$

where $\mathbf{z} \sim \mathcal{N}_{\mathbb{C}}(\mathbf{0}, \sigma^2\mathbf{I}_N)$ while $\mathbf{w} = [w_1, \ldots, w_N]^{\mathrm{T}}$ is such that

$$\mathbf{R}_w = \frac{1}{\sigma_e^2}\mathbb{E}\{\mathbf{w}\mathbf{w}^{\mathrm{H}}\} = \boldsymbol{\Phi}_N\left(\mathbf{R}_{g_m'} \otimes \mathbf{R}_q\right)\boldsymbol{\Phi}_N^{\mathrm{H}} \tag{36}$$

with $\mathbf{R}_q$ being given by (18). The BS estimates the signal s by using the combining vector $\mathbf{v}$ to obtain

$$\hat{s} = \mathbf{v}^{\mathrm{H}}\mathbf{y} = \sqrt{\rho}\mathbf{v}^{\mathrm{H}}\boldsymbol{\Phi}_N\mathbf{x}s + \mathbf{v}^{\mathrm{H}}\mathbf{w} + \mathbf{v}^{\mathrm{H}}\mathbf{z}. \tag{37}$$

To design the combining vector, we adopt the LMMSE criterion that aims to minimize the MSE given by $\mathcal{E}_s = \mathbb{E}\{|\mathbf{v}^{\mathrm{H}}\mathbf{y} - s|^2|\hat{\mathbf{x}}\}$, where $\mathbb{E}\{\cdot|\hat{\mathbf{x}}\}$ denotes the expectation conditioned to the channel estimate $\hat{\mathbf{x}}$. From (37), we obtain

$$\mathcal{E}_s = 1 + \rho\mathbf{v}^{\mathrm{H}}\mathbf{R}_y\mathbf{v} - 2\sqrt{\rho}\Re\mathrm{e}\left(\mathbf{v}^{\mathrm{H}}\boldsymbol{\Phi}_N\hat{\mathbf{x}}\right), \tag{38}$$

with $\mathbf{R}_y = \frac{1}{\rho}\mathbb{E}\{\mathbf{y}\mathbf{y}^{\mathrm{H}}\}$ given by

$$\mathbf{R}_y = \boldsymbol{\Phi}_N\left(\hat{\mathbf{x}}\hat{\mathbf{x}}^{\mathrm{H}} + \mathbf{R}_{\tilde{x}}\right)\boldsymbol{\Phi}_N^{\mathrm{H}} + \frac{\sigma_e^2}{\rho}\mathbf{R}_w + \frac{\sigma^2}{\rho}\mathbf{I}_N. \tag{39}$$

Minimizing (38) with respect to $\mathbf{v}$ yields

$$\mathbf{v} = \frac{1}{\sqrt{\rho}}\mathbf{R}_y^{-1}\boldsymbol{\Phi}_N\hat{\mathbf{x}}, \tag{40}$$

so that the minimum MSE is given by

$$\mathcal{E}_s(\boldsymbol{\phi}) = 1 - \hat{\mathbf{x}}^{\mathrm{H}}\mathbf{Q}(\boldsymbol{\phi})\hat{\mathbf{x}} \tag{41}$$

with

$$\mathbf{Q}(\boldsymbol{\phi}) = \boldsymbol{\Phi}_N^{\mathrm{H}}\mathbf{R}_y^{-1}\boldsymbol{\Phi}_N. \tag{42}$$

Similar to (26), the MSE (41) depends only on $\boldsymbol{\phi}$. An achievable SE can be computed using the so-called hardening capacity bound, which has received great attention in the massive MIMO literature, e.g., [35, Sec. 4.2] since it can be used with any combining scheme and channel estimation method. By adding and subtracting $\sqrt{\rho}\mathbb{E}\left\{\mathbf{v}^{\mathrm{H}}\boldsymbol{\Phi}_N\mathbf{x}\right\}s$, the combined signal $\mathbf{v}^{\mathrm{H}}\mathbf{y}$ can be rewritten as

$$\mathbf{v}^{\mathrm{H}}\mathbf{y} = \sqrt{\rho}\mathbb{E}\left\{\mathbf{v}^{\mathrm{H}}\boldsymbol{\Phi}_N\mathbf{x}\right\}s + \xi, \tag{43}$$

where

$$\xi = \sqrt{\rho}\left(\mathbf{v}^{\mathrm{H}}\boldsymbol{\Phi}_N\mathbf{x} - \mathbb{E}\left\{\mathbf{v}^{\mathrm{H}}\boldsymbol{\Phi}_N\mathbf{x}\right\}\right)s + \mathbf{v}^{\mathrm{H}}\mathbf{w} + \mathbf{v}^{\mathrm{H}}\mathbf{z} \tag{44}$$

has zero mean, i.e., $\mathbb{E}\{\xi\} = 0$ and is uncorrelated with the input s, i.e., $\mathbb{E}\{\xi s^*\} = 0$. In this case, an achievable SE can be obtained as ([35, App. C.3.4])

$$\mathrm{SE} = \frac{\tau_c - \tau}{\tau_c}\log_2\left(1 + \frac{\left|\mathbb{E}\left\{\mathbf{v}^{\mathrm{H}}\boldsymbol{\Phi}_N\mathbf{x}\right\}\right|^2}{\mathbb{E}\{|\xi|^2\}}\right) \tag{45}$$

with

$$\begin{aligned}\mathbb{E}\{|\xi|^2\} =& \mathbb{E}\left\{\left|\mathbf{v}^{\mathrm{H}}\boldsymbol{\Phi}_N\mathbf{x}\right|^2\right\} - \left|\mathbb{E}\left\{\mathbf{v}^{\mathrm{H}}\boldsymbol{\Phi}_N\mathbf{x}\right\}\right|^2 \\ &+ \frac{\sigma_e^2}{\rho}\mathbb{E}\left\{\mathbf{v}^{\mathrm{H}}\mathbf{R}_w\mathbf{v}\right\} + \frac{\sigma^2}{\rho}\mathbb{E}\left\{||\mathbf{v}||^2\right\}\end{aligned} \tag{46}$$

Algorithm 1 The AO outer loop iteration

Input: Desirable accuracy ϵ and the initial phase-shifts $\mathbf{\Phi}_\tau^{(0)}$
Output: Optimized RIS phase-shift matrix $\mathbf{\Phi}_\tau^{\text{opt}}$

Init. initialize $k=0$ and $\Delta_{\mathcal{E}}=1$.
$\mathbf{\Lambda}^{(k+1)} \leftarrow$ substitute $\mathbf{\Phi}_\tau^{(k)}$ into (50);
$\mathcal{E}_x\left(\mathbf{\Lambda}^{(k+1)}, \mathbf{\Phi}_\tau\right) \leftarrow$ substitute $\mathbf{\Lambda}^{(k+1)}$ into (52);
while $\frac{\Delta_{\mathcal{E}}}{\mathcal{E}_x\left(\mathbf{\Lambda}^{(k+1)}, \mathbf{\Phi}_\tau\right)} > \epsilon$ **do**
  $\Delta_{\mathcal{E}} \leftarrow \mathcal{E}_x\left(\mathbf{\Lambda}^{(k+1)}, \mathbf{\Phi}_\tau\right)$;
  Algorithm 2 $\leftarrow \mathbf{\Phi}_\tau^{(k)}$;
  $\mathbf{\Psi}^\star \leftarrow$ Perform Algorithm 2;
  $\mathbf{\Phi}_\tau^{(k+1)} \leftarrow e^{j\angle \mathbf{\Psi}^\star}$;
  $k = k+1$;
  $\mathbf{\Lambda}^{(k+1)} \leftarrow$ substitute $\mathbf{\Phi}_\tau^{(k)}$ into (50);
  $\mathcal{E}_x\left(\mathbf{\Lambda}^{(k+1)}, \mathbf{\Phi}_\tau\right) \leftarrow$ substitute $\mathbf{\Lambda}^{(k+1)}$ into (52);
  $\Delta_{\mathcal{E}} = \mathcal{E}_x\left(\mathbf{\Lambda}^{(k+1)}, \mathbf{\Phi}_\tau\right) - \Delta_{\mathcal{E}}$;
end while
$\mathbf{\Phi}_\tau^{\text{opt}} \leftarrow \mathbf{\Phi}_\tau^{(k)}$.
end procedure

and the expectations are computed with respect to all sources of randomness.

IV. RIS Optimization

We now present an algorithm for designing RIS phase-shifts, which aims to minimize MSE in both the channel estimation and data transmission phases.

A. Optimizing RIS for Channel Estimation

The channel estimation phase is considered first. To minimize the channel estimation error in (26), we can exploit the dependence on $\mathbf{\Phi}_\tau$, and design it to solve the following optimization problem:

$$\min_{\mathbf{\Phi}_\tau \in \mathcal{F}} \ \mathcal{E}_x(\mathbf{\Phi}_\tau) \tag{47}$$

where the feasible set

$$\mathcal{F} = \{\mathbf{\Phi}_\tau \in \mathbb{C}^{\tau \times M} | \ |[\mathbf{\Phi}_\tau]_{i,m}| = 1; \forall i, m\} \tag{48}$$

captures the fact that the RIS is a passive device whose coefficients must have unitary modulus.

The optmization problem (47) is not convex in $\mathbf{\Phi}_\tau$ and finding its solution involves the optimization over large matrices. To solve it, we rewrite (26) as

$$\mathcal{E}_x(\mathbf{\Phi}_\tau) = \text{tr}\left\{\mathbf{R}_x - \mathbf{\Lambda}(\mathbf{\Phi}_\tau)\mathbf{\Phi}_{N\tau}\mathbf{R}_x\right\}, \tag{49}$$

with

$$\mathbf{\Lambda}(\mathbf{\Phi}_\tau) = \mathbf{R}_x \mathbf{\Phi}_{N\tau}^{\text{H}} \left(\mathbf{R}_y^{\text{tr}}\right)^{-1}. \tag{50}$$

Moreover, we make a simplifying assumption, that is, we neglect the fact that $\mathbf{\Lambda}(\mathbf{\Phi}_\tau)$ depends on the value of $\mathbf{\Phi}_\tau$. Hence, we rewrite the objective function in (47) as

$$\mathcal{E}_x(\mathbf{\Phi}_\tau) = \mathcal{E}_x(\mathbf{\Lambda}, \mathbf{\Phi}_\tau), \tag{51}$$

as if $\mathbf{\Lambda}$ and $\mathbf{\Phi}_\tau$ were independent variables. Under this hypothesis, (47) can be solved by following an AO approach to alternately optimize $\mathbf{\Lambda}$ and $\mathbf{\Phi}_\tau$. The AO is an iterative algorithm whose key advantage is that it simplifies the optimization process by breaking it into smaller subproblems, which are easier to solve. The AO approach is especially helpful when the original problem involves complicated interactions or dependencies among the variables. In particular, we propose a two-step *iterative* algorithm, where $\mathcal{E}_x$ is alternatively optimized with respect to $\mathbf{\Lambda}$ and $\mathbf{\Phi}_\tau$. Being $\mathbf{\Lambda}^{(k)}$ and $\mathbf{\Phi}_\tau^{(k)}$ the values found at iteration k, at iteration $k+1$ we proceed as follows:

1) Having fixed the value of $\mathbf{\Phi}_\tau = \mathbf{\Phi}_\tau^{(k)}$, we minimize (51) by computing $\mathbf{\Lambda}^{(k+1)}$ as $\mathbf{\Lambda}(\mathbf{\Phi}_\tau)$ in (50). This optimization is unconstrained and is a straightforward application of MSE minimization;
2) Fixing $\mathbf{\Lambda} = \mathbf{\Lambda}^{(k+1)}$, the MSE takes the expression given in

$$\begin{aligned}\mathcal{E}_x\left(\mathbf{\Lambda}, \mathbf{\Phi}_\tau\right) &= \text{tr}\left\{\mathbf{\Lambda}\mathbf{R}_y^{\text{tr}}\mathbf{\Lambda}^{\text{H}} - 2\Re\left[\mathbf{\Lambda}\mathbf{\Phi}_{N\tau}\mathbf{R}_x\right] + \mathbf{R}_x\right\} \\ &= \text{tr}\left\{\mathbf{\Lambda}\left(\mathbf{\Phi}_{N\tau}\mathbf{R}_x\mathbf{\Phi}_{N\tau}^{\text{H}} + \frac{\sigma_e^2}{\rho^{\text{tr}}}\mathbf{R}_w^{\text{tr}} + \frac{\sigma^2}{\rho^{\text{tr}}}\mathbf{I}_{N\tau}\right)\mathbf{\Lambda}^{\text{H}}\right. \\ &\left. -\mathbf{\Lambda}\mathbf{\Phi}_{N\tau}\mathbf{R}_x - \mathbf{R}_x\mathbf{\Phi}_{N\tau}^{\text{H}}\mathbf{\Lambda}^{\text{H}} + \mathbf{R}_x\right\}\end{aligned} \tag{52}$$

and $\mathcal{E}_x(\mathbf{\Lambda}, \mathbf{\Phi}_\tau)$ is now a *convex* function of $\mathbf{\Phi}_\tau$. The RIS phase-shift matrix is computed as the solution of the minimization

$$\mathbf{\Phi}_\tau^{(k+1)} = \arg\min_{\mathbf{\Phi}_\tau \in \mathcal{F}} \mathcal{E}_x\left(\mathbf{\Lambda}^{(k+1)}, \mathbf{\Phi}_\tau\right). \tag{53}$$

Regarding the convergence of the above algorithm we can observe that, since in both steps we minimize the MSE, at each iteration the MSE either decreases or reaches a point where it remains unchanged. Given that the MSE is a positive value, the procedure will ultimately converge to a local optimum. In the remainder of the paper, we will mention the iterations of the AO algorithm as *outer loop* iterations.

1) Solving (53) *via Projected Gradient Method:* Although the objective function in (53) is convex with respect to $\mathbf{\Phi}_\tau$, the optimization problem is still non-convex due to the presence of the unitary modulus constraint. Given the simplicity of projecting any solution onto the feasible set $\mathcal{F}$, this type of constraint leads to the use of the *projected gradient* (PG) method. The PG is an iterative algorithm, which, although sub-optimal, is effective and shows fast convergence towards a local optimum. The idea is to employ gradient descent, iterated until convergence, to solve the unconstrained problem and then project the solution on the feasible set $\mathcal{F}$. In practice, we need to introduce an extra auxiliary loop variable $\mathbf{\Psi}^{(s)}$ to describe the intermediate RIS coefficients during gradient descent. The application of the PG method requires to define the gradient and Hessian of the complex matrix (52), which are given in Appendix B.

After that, the PG algorithm is initialized by setting $\mathbf{\Psi}^{(0)} = \mathbf{\Phi}_\tau^{(k)}$, the last solution of the AO algorithm, then the two steps of the PG method are:

1) Compute the unconstrained RIS coefficient matrix by solving the unconstrained problem via gradient descent. Employing the gradient (75) in Appendix B, $\mathbf{\Psi}^{(s)}$ is

Algorithm 2 The PG inner loop iteration

Input: Desirable accuracy ε, step size α and $\mathbf{\Phi}_\tau^{(k)}$
Output: $\mathbf{\Psi}^\star$

Init. initialize $s=0$, $\mathbf{\Psi}^{(s)}=\mathbf{\Phi}_\tau^{(k)}$ and $\Delta_\Psi=1$.
while $\Delta_\Psi>\varepsilon$
  $\mathbf{G}^{(s)}\leftarrow\nabla_{\mathbf{\Psi}}\mathcal{E}_x\left(\mathbf{\Lambda},\mathbf{\Psi}^{(s)}\right)$ via (75);
  $\Delta_\Psi\leftarrow\|\mathbf{G}^{(s)}\|$;
  $\mathbf{D}^{(s)}\leftarrow\left(\nabla^2_{\mathbf{\Psi}}\mathcal{E}_x\left(\mathbf{\Lambda},\mathbf{\Psi}^{(s)}\right)\odot\mathbf{I}_{\tau M}\right)^{-1}$ via (79);
  $\left[\mathbf{\Psi}^{(s+1)}\right]_{i,m}\leftarrow\left[\mathbf{\Psi}^{(s)}\right]_{i,m}-\frac{\alpha\left[\mathbf{G}^{(s)}\right]_{(m-1)\tau+i}}{\left[\mathbf{D}^{(s)}\right]_{(m-1)\tau+i,(m-1)\tau+i}}$;
  $s=s+1$;
end while
$\mathbf{\Psi}^\star\leftarrow\mathbf{\Psi}^{(s)}$;
end procedure

updated as

$$\left[\mathbf{\Psi}^{(s+1)}\right]_{i,m}=\left[\mathbf{\Psi}^{(s)}\right]_{i,m}-\alpha\left[\mathbf{D}^{(s)}\nabla_{\mathbf{\Psi}}\mathcal{E}_x\left(\mathbf{\Lambda},\mathbf{\Psi}^{(s)}\right)\right]_z, \tag{54}$$

where $\mathbf{D}^{(s)}\in\mathbb{C}^{\tau M\times\tau M}$ is an Hermitian positive definite matrix and the value of $\mathbf{\Lambda}$ is the outcome of the previous outer loop AO iteration. We denote with $\mathbf{\Psi}^\star$ the matrix obtained at convergence.

2) Project $\mathbf{\Psi}^\star$ onto $\mathcal{F}$, by normalizing the amplitude of each entry to unity, i.e.[4],

$$\mathbf{\Phi}_\tau^{(k+1)}=e^{j\angle\mathbf{\Psi}^\star}. \tag{55}$$

2) Solving (54) *via Newton's Method:* Gradient descent is iterative by nature and (54) may need to be iterated several times before achieving convergence, so that the speed of convergence and the choice of the stepsize α are important issues for this type of iterative methods. In particular, when the Hessian of the objective function is known, we can choose

$$\mathbf{D}^{(s)}=\left(\nabla^2_{\mathbf{\Psi}}\mathcal{E}_x\left(\mathbf{\Lambda},\mathbf{\Psi}^{(s)}\right)\right)^{-1}. \tag{56}$$

In this case, the iterative algorithm is indicated as the *Newton*'s method and has the great advantage of being able to find the minimum of a quadratic function as (52) with very few iterations [36]. From Appendix B, for the single-input and single-output (SISO) case the Hessian is

$$\nabla^2_{\mathbf{\Psi}}\mathcal{E}_x\left(\mathbf{\Lambda},\mathbf{\Psi}\right)=2\mathbf{\Lambda}^{\mathrm{H}}\mathbf{\Lambda}\otimes\mathbf{R}_c+\frac{2\sigma_e^2}{\rho^{\mathrm{tr}}}\left(\left(\mathbf{\Lambda}^{\mathrm{H}}\mathbf{\Lambda}\right)\odot\mathbf{I}_\tau\right)\otimes\mathbf{R}_q, \tag{57}$$

and we can conclude that the elements in the diagonal of $\nabla^2_{\mathbf{\Psi}}\mathcal{E}_x$ are all positive, being obtained as products of positive factors. It can be shown that the same property applies also to the multiple-input single-output (MISO) case. Accordingly, considered the potentially high computational complexity of inverting the $\tau M\times\tau M$ Hessian matrix, a simplified version of the Newton's method, which is valid when the elements on the diagonal of the Hessian are all strictly positive, is obtained by approximating the Hessian by the elements of its main diagonal, so that it is

$$\mathbf{D}^{(s)}=\left(\nabla^2_{\mathbf{\Psi}}\mathcal{E}_x\left(\mathbf{\Lambda},\mathbf{\Psi}^{(s)}\right)\odot\mathbf{I}_{\tau M}\right)^{-1}. \tag{58}$$

In this specific case, the update rule for the *diagonally scaled steepest descent* method takes the form

$$\left[\mathbf{\Psi}^{(s+1)}\right]_{i,m}=\left[\mathbf{\Psi}^{(s)}\right]_{i,m}-\frac{\alpha\left[\nabla_{\mathbf{\Psi}}\mathcal{E}_x\right]_{(m-1)\tau+i}}{\left[\nabla^2_{\mathbf{\Psi}}\mathcal{E}_x\right]_{(m-1)\tau+i,(m-1)\tau+i}}. \tag{59}$$

The AO outer and PG inner loop iterations for alternating optimization $\mathbf{\Lambda}$ and $\mathbf{\Phi}_\tau$ are summarized in Algorithm 1 and Algorithm 2, respectively.

[4]The projection method used is required to be designed based on the feasible set of RIS phase-shifts. When the RIS phase-shifts are discrete, the minimization of the Euclidean distance criterion can be applied to obtain the optimal solution within the feasible set.

Algorithm 3 Optimization of $\boldsymbol{\phi}$ during the transmission part

Input: Desirable accuracy ξ, and the initial phase-shifts $\boldsymbol{\phi}^{(0)}$
Output: Optimized RIS phase-shifts $\boldsymbol{\phi}_{\text{opt}}$

Init. initialize $k=0$ and $\Delta_\mathcal{E}=1$.
$\mathbf{v}^{(k+1)}\leftarrow$ substitute $\boldsymbol{\phi}^{(k)}$ into (40);
$\mathcal{E}_s(\mathbf{v}^{(k+1)},\boldsymbol{\phi};\hat{\mathbf{x}})\leftarrow$ substitute $\mathbf{v}^{(k+1)}$ into (38);
while $\frac{\Delta_\mathcal{E}}{\mathcal{E}_s(\mathbf{v}^{(k+1)},\boldsymbol{\phi};\hat{\mathbf{x}})}>\xi$ **do**
  $\Delta_\mathcal{E}\leftarrow\mathcal{E}_s(\mathbf{v}^{(k+1)},\boldsymbol{\phi};\hat{\mathbf{x}})$;
  $\boldsymbol{\theta}^\star\leftarrow$ Apply the PG method for (61);
  $\boldsymbol{\phi}^{(k+1)}\leftarrow e^{j\angle\boldsymbol{\theta}^\star}$;
  $k=k+1$;
  $\mathbf{v}^{(k+1)}\leftarrow$ substitute $\boldsymbol{\phi}^{(k)}$ into (40);
  $\mathcal{E}_s(\mathbf{v}^{(k+1)},\boldsymbol{\phi};\hat{\mathbf{x}})\leftarrow$ substitute $\mathbf{v}^{(k+1)}$ into (38);
  $\Delta_\mathcal{E}=\mathcal{E}_s(\mathbf{v}^{(k+1)},\boldsymbol{\phi};\hat{\mathbf{x}})-\Delta_\mathcal{E}$;
end while
$\boldsymbol{\phi}_{\text{opt}}\leftarrow\boldsymbol{\phi}^{(k)}$.
end procedure

B. Optimizing RIS for Data Transmission

In the following, we consider the RIS phase-shift design for the data transmission phase. This phase-shift would be alternately optimized with the combiner at the BS following steps similar to those in Algorithms 1 and 2. To proceed further, we rewrite (41) as a function of $\mathbf{v}$ and $\boldsymbol{\phi}$ and formulate the optimization problem as follows:

$$\min_{\boldsymbol{\phi}}\ \mathcal{E}_s(\mathbf{v},\boldsymbol{\phi};\hat{\mathbf{x}}),\ \text{ s.t. }\ |[\boldsymbol{\phi}]_m|=1. \tag{60}$$

Considered that also $\mathbf{R}_y$ depends on $\boldsymbol{\phi}$, $\mathcal{E}_s(\mathbf{v},\boldsymbol{\phi};\hat{\mathbf{x}})$ is a non-convex function of $\boldsymbol{\phi}$ and to solve (60) we can follow once again the *AO* approach.

Let $\boldsymbol{\phi}^{(k)}$ be the vector of RIS coefficients at iteration k, then $\mathbf{v}^{(k+1)}$ is computed by replacing $\mathbf{\Phi}_N$ with $\mathbf{I}_N\otimes{\boldsymbol{\phi}^{(k)}}^{\mathrm{T}}$ in (40). The new vector of RIS coefficients $\boldsymbol{\phi}^{(k+1)}$ can be found by solving

$$\begin{aligned}\boldsymbol{\phi}^{(k+1)}=\arg\min_{\boldsymbol{\phi}}\ &\mathcal{E}_s(\mathbf{v}^{(k+1)},\boldsymbol{\phi};\hat{\mathbf{x}}),\\ &\text{s.t. }\ |[\boldsymbol{\phi}]_m|=1,\end{aligned} \tag{61}$$

and it can be solved by applying the PG method, with the required gradient and Hessian provided in (82) and (83) of Appendix B. Then, the specific steps to obtain $\boldsymbol{\phi}_{\text{opt}}$ are summarized in Algorithm 3. Since the MSE decreases at each

TABLE I: The Computational Complexity of Solving (60).

Step	Complexity	
$\mathbf{R}_y$	$\mathcal{O}(M^2N^3)$	
AO	$\mathbf{v}^{(k+1)}$	$\mathcal{O}(MN^3)$
	$\mathcal{E}_s(\mathbf{v}^{(k+1)}, \boldsymbol{\phi}; \hat{\mathbf{x}})$	$\mathcal{O}(MN^2)$
PG	Gradient	$\mathcal{O}(M^3N^3)$
	Hessian	$\mathcal{O}(M^3N^3)$

iteration until it reaches a point where it remains unchanged, the procedure necessarily converges to a local optimum.

C. Optimization Execution and Complexity Discussion

As illustrated by Algorithms 1 and 2, the RIS phase-shift $\boldsymbol{\Phi}_\tau$ used during the training phase is alternately optimized with the LMMSE estimator $\boldsymbol{\Lambda}(\boldsymbol{\Phi}_\tau)$, utilizing only known correlation matrices $\mathbf{R}_x$ and $\mathbf{R}_w^{\text{tr}}$, without requiring any online information. Consequently, the RIS phase-shift used during the training phase can be designed offline without consuming any channel uses. Leveraging this phase-shift, the optimal LMMSE estimate $\hat{\mathbf{x}}$ of the cascade channel can be obtained online according to (22). Subsequently, as depicted by Algorithm 3, the RIS phase-shift[5] used for uplink online data transmission is optimized based on the estimate $\hat{\mathbf{x}}$ and the second-order statistics $\mathbf{R}_x$ and $\mathbf{R}_w$. Finally, the combined signal $\hat{s}$ is obtained at the BS based on (43) by utilizing the optimal LMMSE combiner $\mathbf{v}(\boldsymbol{\phi}_{\text{opt}})$. In general, when the spatial correlation matrices $\mathbf{R}_x$ and $\mathbf{R}_w$ (also $\mathbf{R}_w^{\text{tr}}$) remain constant, the proposed MMSE solution can be continuously applied in the RIS-aided communication with EMI. However, if the required second-order statistics change, it is necessary to remeasure them before executing the MMSE solution.

Considering that the optimization of RIS phase-shifts used during the data transmission phase relies on the online estimate $\hat{\mathbf{x}}$, we evaluate the computational complexity of this process here, as shown in Table I. Before executing optimization Algorithm 3, the covariance $\mathbf{R}_y = \frac{1}{\rho}\mathbb{E}\{\mathbf{y}\mathbf{y}^{\text{H}}\}$ needs to be computed first according to (39). The complexity of this process is $\mathcal{O}(M^2N^3)$, primarily arising from matrix multiplication. Then, following Algorithm 3, during the AO outer loop iteration, the computational complexity of calculating $\mathbf{v}^{(k+1)}$ and $\mathcal{E}_s(\mathbf{v}^{(k+1)}, \boldsymbol{\phi}; \hat{\mathbf{x}})$ is $\mathcal{O}(MN^3)$ and $\mathcal{O}(MN^2)$, respectively. While during the PG inner loop iteration, the computational complexity mainly comes from computing the gradient and Hessian of $\mathcal{E}_s(\mathbf{v}^{(k+1)}, \boldsymbol{\theta}; \hat{\mathbf{x}})$, both with complexity $\mathcal{O}(M^3N^3)$. Considering the significant number of elements in the practical RIS, the computational complexity during the PG inner loop iteration is much higher than that during the AO outer loop iteration. Therefore, in the practical application of the proposed approach, it may be advantageous to execute the gradient descent only once within the inner loop iteration. This may result in an increase in the number of AO outer loop iteration, but overall, it can accelerate the convergence speed of the proposed method.

[5]Due to the significant shift in the role of EMI, this RIS phase-shift cannot be directly applied to the downlink transmission. However, similar to the steps in Algorithm 3, the optimal RIS phase-shift for the downlink can be obtained through alternating optimization of the LMMSE detector at the UE and the RIS phase-shift.

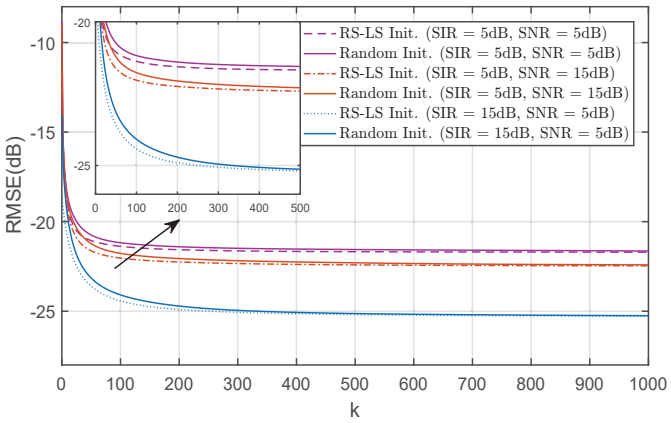

Fig. 3: The RMSEs vs. k for the LMMSE estimator with AO.

V. Numerical Results

Numerical results are now given to verify the performance of the proposed channel estimation and transmission schemes. We begin by considering a SISO scenario, with the exception of Fig. 4 (b). The required gradient and Hessian matrices in the SISO case are provided in Appendix B. Unless otherwise stated, the RIS is equipped with $M = 36$ elements with $M_H = M_V = 6$, and the vertical and horizontal inter-element distances are set to $\lambda/2$. The pilot length is set to $\tau = M = 36$ and the coherence interval is $\tau_c = 10\tau = 360$ symbols.

A. Channel Estimation Analysis

The accuracy of the channel estimators is evaluated in terms of the relative MSE (RMSE), defined as $\mathbb{E}\{\|\mathbf{x} - \hat{\mathbf{x}}\|^2/M\}$. The scattering function $f_h(\varphi, \vartheta)$ in the spatial correlation matrix $\mathbf{R}_h$ for the UE-RIS channel follows the Gaussian distribution within the $\triangle_h = 10^\circ$ neighborhood of $(\varphi_h, \vartheta_h) = (70^\circ, -20^\circ)$, and the scattering function $f_{g_n}(\varphi, \vartheta)$ in $\mathbf{R}_{g_n}$ also follows the Gaussian distribution within the $\triangle_{g_n} = 5^\circ$ neighborhood of $(\varphi_{g_n}, \vartheta_{g_n}) = (-60^\circ, -30^\circ)$. The scattering function $f_e(\varphi, \vartheta)$ in $\mathbf{R}_e$ for the EMI is selected the Gaussian distribution within the $\triangle_e = 20^\circ$ neighborhood of $(\varphi_e, \vartheta_e) = (-10^\circ, 20^\circ)$, as illustrated in Table II.

We explore three different approaches in this part:

1) The first is the proposed AO approach for minimizing MSE, defined in Algorithms 1 and 2 and simply referred to as 'MMSE' in the figures.
2) The second is the RS-LS estimator defined in (30), where the RIS is optimized based on [6]. The RIS

TABLE II: Simulation parameters.

Cascaded Channel				EMI	
φ_h	ϑ_h	φ_{g_n}	ϑ_{g_n}	φ_e	ϑ_e
70°	-20°	-60°	-30°	-10°	20°
$\triangle_h = 10^\circ$		$\triangle_{g_n} = 5^\circ$		$\triangle_e = 20^\circ$	
$\{f_i(\varphi, \vartheta) \mid i = g_n, h, e\}$: Gaussian Model					

This article has been accepted for publication in IEEE Transactions on Wireless Communications. This is the author's version which has not been fully edited and content may change prior to final publication. Citation information: DOI 10.1109/TWC.2024.3449074

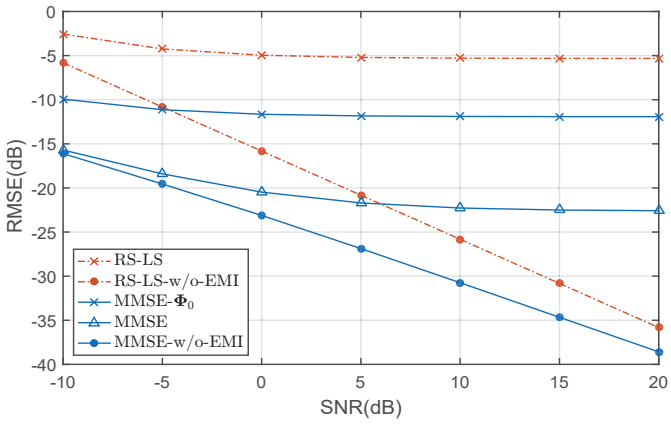

(a)

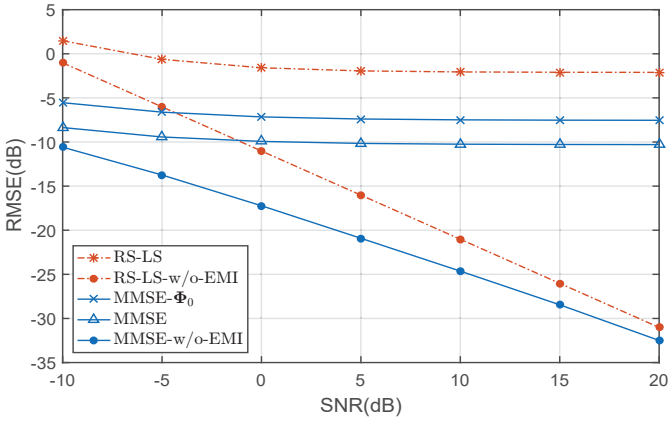

(b)

Fig. 4: The RMSEs vs. SNR for different estimators and RIS phase-shift configurations. (a) SISO case. (b) MISO case.

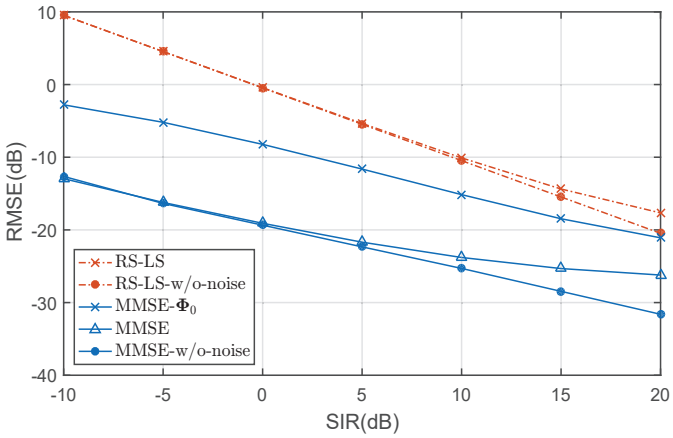

Fig. 5: The RMSEs vs. SIR for different estimators and RIS phase-shift configurations.

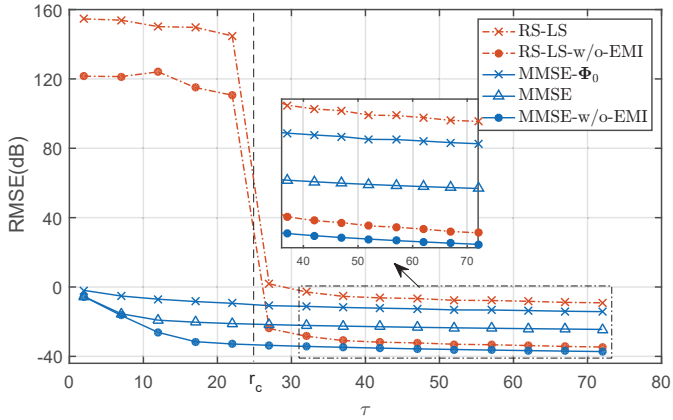

Fig. 6: The RMSEs vs. τ for different estimators and RIS phase-shift configurations.

configuration obtained by RS-LS is denoted as $\mathbf{\Phi}_0$ and used as the initial phase in Algorithm 1.

3) The third approach is referred to as 'MMSE-$\mathbf{\Phi}_0$', where the RIS shifts are $\mathbf{\Phi}_0$, but unlike RS-LS, the linear filter is calculated as in (50), i.e., based on the LMMSE criterion.

Besides, we assume $\alpha = 0.5$ and $\epsilon = 10^{-5}$ for the proposed approach, and to improve simulation speed, we apply the diagonally scaled steep descent method only once within the inner loop iteration defined in Algorithm 2.

Fig. 3 depicts the RMSE of the LMMSE estimator with the AO algorithm as a function of the outer iteration count k under varying SNRs and SIRs. The abbreviation 'RS-LS Init.' signifies that the AO algorithm is initiated with $\mathbf{\Phi}_0$, the optimal phase-shifts for the RS-LS estimator. In contrast, 'Random Init.' denotes the initialization of the AO algorithm with random unit-modulus phase-shifts. As detailed in Section IV, the AO algorithm converges progressively as k increases. Notably, the AO algorithm exhibits slightly faster convergence when initialized with $\mathbf{\Phi}_0$ compared to when initialized with random unit-modulus phase-shifts. This observation motivates our choice to employ the $\mathbf{\Phi}_0$ initialization in the forthcoming simulations.

Fig. 4 shows the RMSE as a function of SNR when SIR $= 5$ dB both in the SISO and MISO scenarios. In the MISO case, the UPA at the BS consists of 2×2 antennas. For comparison purposes, we also show the results of 'MMSE' and 'RS-LS' schemes when SIR $= \infty$, i.e. EMI is not present, which are denoted 'w/o EMI'. Let us first consider the case where the RIS is not affected by interference. In this case, both the LMMSE and RS-LS estimators show linearly decreasing MSE with SNR. Also, LMMSE outperforms RS-LS especially at low SNRs, which is consistent with expectations for MMSE estimation compared to LS. In the presence of EMI, a threshold approximately corresponding to SNR = SIR is observed in all cases, i.e., when SIR begins to be the predominant effect. Moreover, 'MMSE-$\mathbf{\Phi}_0$' outperforms the RS-LS method by almost 5 dB, even though both methods use the same RIS configuration $\mathbf{\Phi}_0$. This is because, in the MMSE case, the LMMSE criterion takes into account both noise and EMI statistics. More importantly, the proposed 'MMSE' scheme provides consistent gain in terms of 'MMSE-$\mathbf{\Phi}_0$', which proves the effectiveness of the proposed iterative RIS optimization approach in Algorithms 1 and 2. Finally, comparing Fig. 4 (a) and Fig. 4 (b), in the MISO scenario, all estimators exhibit consistency in performance with those in the SISO scenario. However, due to the increased channel dimension that needs to be estimated, their overall performance is slightly inferior to the estimators in the SISO scenario.

Fig. 5 shows the RMSE as a function of SIR at an SNR of 5 dB. The performance of all algorithms shows similar behavior as in the previous case, with the difference that the

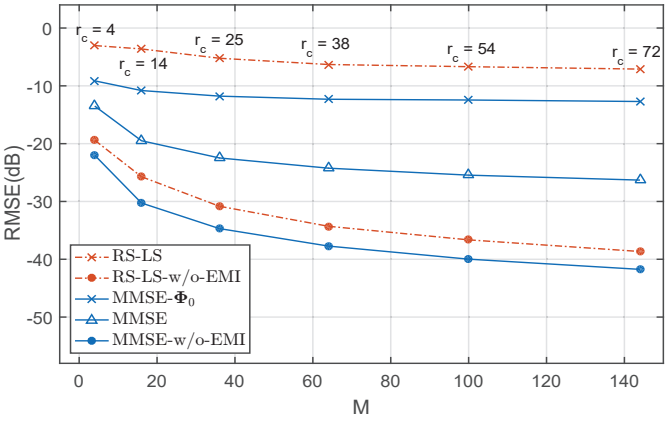

Fig. 7: The RMSEs vs. M for different estimators and RIS phase-shift configurations.

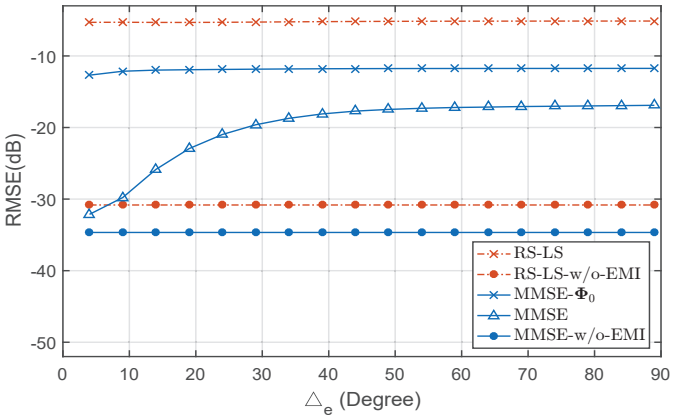

Fig. 8: The RMSEs vs. $\triangle_e$ for different estimators and RIS phase-shift configurations.

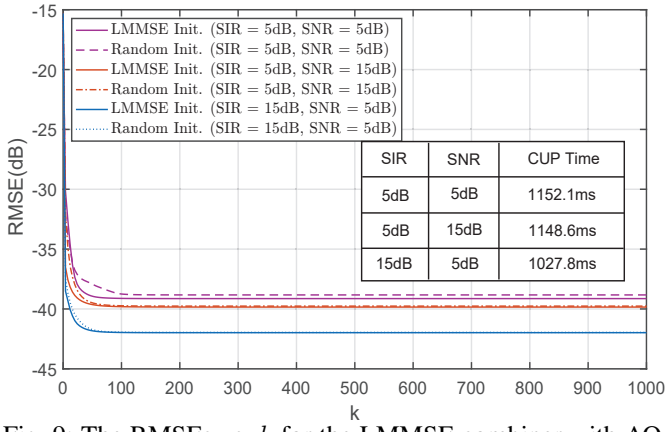

Fig. 9: The RMSEs vs. k for the LMMSE combiner with AO.

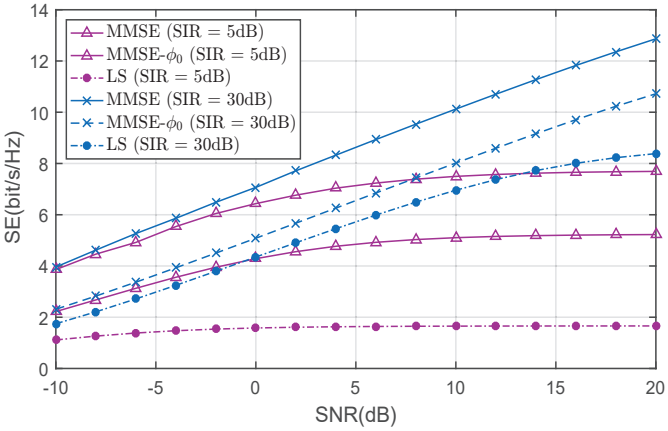

Fig. 10: The achievable SE vs. SNR for different combiners.

threshold appears for SIR $\gg$ SNR, indicating that EMI is the most detrimental effect for channel estimation. As before, the best results are obtained with the proposed LMMSE estimator, and this behavior is more evident for low SIR, i.e., when the impact of EMI is higher. Specifically, the performance gap between 'RS-LS' and 'MMSE' at SIR $=$ 20 dB is of 8.55 dB, whereas the gap increases to 18.65 dB at SIR $=$ 0 dB.

Fig. 6 shows the RMSE as a function of the pilot length τ when SNR $=$ 15 dB and SIR $=$ 5 dB. We show in the figure $r_c = \text{rank}\{\mathbf{R}_c\}$, which is the minimum number of pilots that can be used by the RS-LS scheme according to [6]. It can be seen from the figure that the LMMSE estimator can be applied for any $\tau \geq 1$, but naturally improves its performance as τ increases. The largest performance improvement is observed for $\tau < r_c$, while the performance tends to reach a threshold as τ approaches the number of RIS elements M. Conversely, as expected, the performance of the RS-LS estimator for $\tau < r_c$ is very poor due to the insufficient number of pilots. Also in this case, the performance tends to stabilize as τ approaches M.

Fig. 7 shows the RMSE as a function of M at SNR = 15dB and SIR $=$ 5 dB. Note that increasing M increases the number of pilots to be estimated. However, this has only a limited effect on the channel rank, i.e., on the effective channel dimension. Thus, the main effect is to increase the RIS gain, which is beneficial for channel estimation. Accordingly, the RMSE value of both estimators decreases as M increases. It is also worth noting that the difference in performance between 'MMSE' and 'RS-LS' increases with M.

So far, we have assumed that the interference and the pilot signals come from different directions and do not overlap. In Fig. 8, we evaluate the RMSE as a function of angular spread, considering $\triangle_e$ from $4°$ to $89°$. The SNR and SIR are both set to 15 dB. As expected, the gap between 'MMSE' and 'MMSE-w/o-EMI' increases as $\triangle_e$ increases. When the interference approaches isotropic scattering, i.e., $\triangle_e \geq 50°$, the gap between the two curves reaches 17.34 dB. This is due to the physical overlap between the UE-RIS channel $\mathbf{h}$ and the interference $\mathbf{e}(i)$. Since only the signal subspace under the assumption of isotropic conditions is used to design $\mathbf{\Phi}_0$ [6], the estimators 'MMSE-$\mathbf{\Phi}_0$' and 'RS-LS' are less sensitive to changes in $\triangle_e$ compared to the 'MMSE' estimator. However, even in the isotropic case, the 'MMSE' estimator still retains a performance advantage of about 11.78 dB over the RS-LS estimator.

B. Spectral Efficiency Analysis

We now consider the data transmission phase using the correlated Rayleigh model as an example. We consider two approaches:

1) The first one is the proposed LMMSE combiner with AO defined in Algorithm 3, labeled as 'MMSE'. The

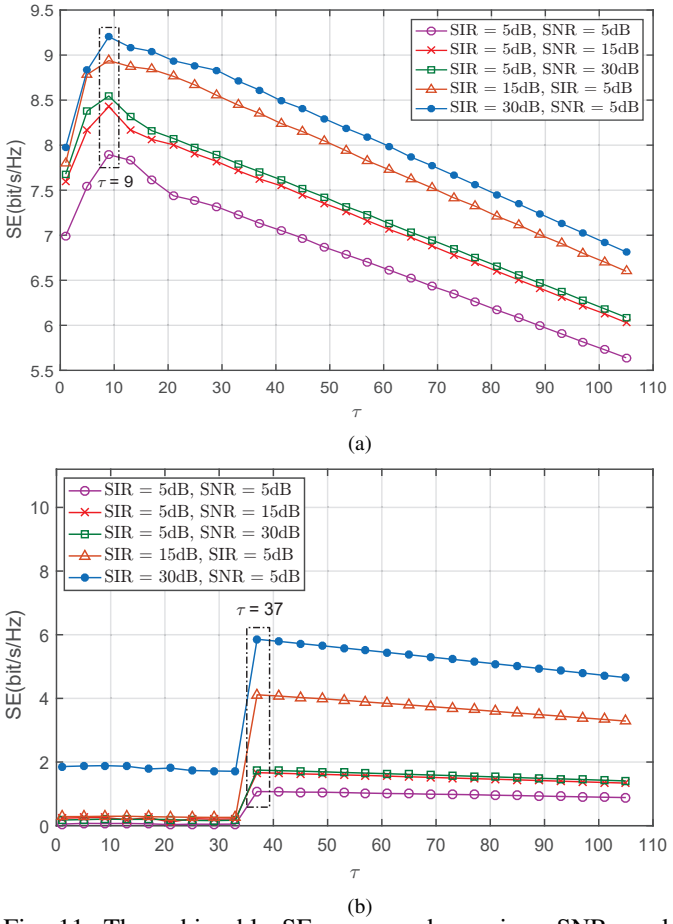

Fig. 11: The achievable SE vs. τ under various SNRs and SIRs. (a) The LMMSE combiner. (b) The LS combiner.

initial ϕ_0 for the AO algorithm is set to a row of $\mathbf{\Phi}_\tau^{\text{opt}}$, the optimal phase-shifts for the LMMSE estimator.

2) Additionally, the conventional LS combiner $\mathbf{v}_{\text{LS}} = \frac{1}{\rho}\mathbf{\Phi}_N\hat{\mathbf{x}}\left(\hat{\mathbf{x}}^{\text{H}}\mathbf{\Phi}_N^{\text{H}}\mathbf{\Phi}_N\hat{\mathbf{x}}\right)^{-1}$ is provided as a reference, which is designed based on the RS-LS estimate as shown in (30). In the LS scheme, the RIS phase-shift $\mathbf{\Phi}_\tau^{\text{RS-LS}}$ for the RS-LS estimator is still computed based on [6], while during the data transmission phase, the RIS phase-shift for the LS combiner is selected as a row of $\mathbf{\Phi}_\tau^{\text{RS-LS}}$.

Fig. 9 depicts the RMSE of the LMMSE combiner with the AO algorithm as a function of the outer iteration count k. We provide two initial RIS phase-shifts for the AO algorithm: one is a row of $\mathbf{\Phi}_\tau^{\text{opt}}$ mentioned above, denoted as 'LMMSE. Init.', and the other is set to the random unit-modulus phase-shifts, labeled as 'Random Init.'. To reflect the computational complexity, the CPU times of the curves initialized with 'LMMSE. Init.' is provided in Fig. 9. It can be observed that the AO algorithm takes approximately 1000 ms to iterate $k = 1000$ times, but this also depends on the processor used. Furthermore, consistent with the conclusion of Fig. 3, the AO algorithm initialized with 'LMMSE. Init.' exhibits slightly faster convergence compared to that initialized with the random unit-modulus phase-shifts. Therefore, for the subsequent simulations, AO algorithm is initialized with the row of $\mathbf{\Phi}_\tau^{\text{opt}}$.

Fig. 10 presents the SE as a function of SNR, in which the LMMSE combiner with ϕ_0 is provided as a benchmark. When the RIS is almost unaffected by white interference, i.e., SIR $=$ 30dB, the SE of all combiners exhibits nearly linear growth with increasing SNR. In the presence of EMI, a threshold slightly above SNR $=$ SIR can be observed in all combiners. This indicates that the EMI is the most adverse factor inhibiting SE in the data transmission phase. Moreover, due to the adoption of the LMMSE criterion, which considers both noise and EMI statistics, even when only employing initial RIS phase-shifts ϕ_0, 'MMSE-ϕ_0' outperforms the conventional LS combiner. Furthermore, after employing the AO algorithm, the performance of the LMMSE combiner is improved by over 2 bits/s/Hz compared to 'MMSE-ϕ_0'. This underlines the effectiveness of the AO algorithm in the transmission part.

Fig. 11 depict the SE as a function of pilot length τ for LMMSE combiner and LS combiner, where the pilot length is set in the range 1 to $\tau_{\max} = 3M = 108$. It can be seen that for both combiners, the SE does not monotonically vary with τ. Specifically, for the LS combiner, when $\tau < M$, due to the poor performance of the RS-LS estimator, as shown in Fig. 6, the SE of the LS combiner is very poor. Subsequently, when $\tau > M$, the accuracy of the RS-LS estimator does not significantly improve with the increase of τ. In this case, additional pilot sequences would consume the avaiable coherence interval τ_c, leading to a decrease in the SE. The same conclusion can also be drawn for the proposed LMMSE scheme, namely, when $\tau > 9$, the unnecessary pilot overhead would decrease the SE. Therefore, a compromise design of the pilot length is crucial for achieving the optimal SE in RIS-aided communications. More importantly, comparing Fig. 11 (a) and Fig. 11 (b), we can conclude that the proposed LMMSE scheme outperforms the conventional LS method in both SE and required pilot length. This demonstrates the superiority of the proposed scheme.

C. Performance Comparison for Different Channel Models

We now evaluate the performance of the proposed MMSE approach with AO in the correlated Rayleigh, Rician, and LoS channel scenarios to validate its general applicability. Fig. 12 first presents the RMSE of the LMMSE estimator for different channel models as a function of SNR at SIR $=$ 10 dB. It is evident that the proposed LMMSE estimator demonstrates outstanding performance, particularly in the LoS channel, where its RMSE closely matches that of the 'MMSE-w/o-EMI' case. The Rician channel follows closely behind, while the performance in the correlated Rayleigh channel is relatively poorer. Despite this, the proposed LMMSE estimator, guided by the the minimum MSE criterion, achieves an RMSE below -15 dB for the Rayleigh channel, indicating acceptable performance. Additionally, after utilizing the proposed AO method, the 'MMSE' method achieves gains of 14.93 dB, 11.26 dB, and 10.27 dB for the LoS, Rician, and correlated Rayleigh channels, respectively, compared to the 'MMSE-$\mathbf{\Phi}_0$' method.

Fig. 13 depicts the SE of the LMMSE combiner for the aforementioned three channels as a function of SNR at SIR

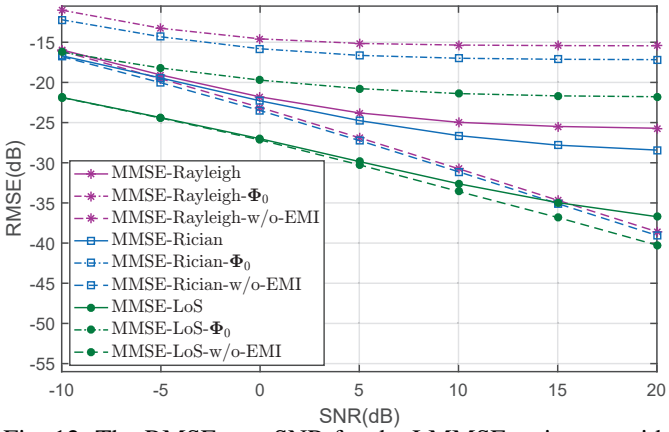

Fig. 12: The RMSEs vs. SNR for the LMMSE estimator with different channel models.

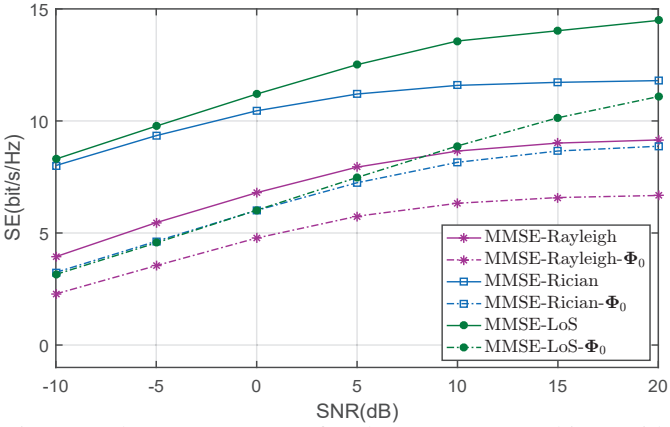

Fig. 13: The SEs vs. SNR for the LMMSE combiner with different channel models.

$= 10$ dB. As expected, the LMMSE combiner shows the best SE for the LoS channel, followed by the Rician channel, with the correlated Rayleigh channel performing slightly worse. Additionally, the proposed AO method provides the performance improvements of 3.40 bits/s/Hz, 2.93 bits/s/Hz, and 2.48 bits/s/Hz for the LoS, Rician, and correlated Rayleigh channels, respectively. Combining the results from Fig. 12 and Fig. 13, it is robustly verified that the designed MMSE scheme is applicable to the correlated Rayleigh, Rician, and LoS channel scenarios.

VI. Conclusions

This paper focuses on a RIS-based system in which a single-antenna UE exchanges information with a multi-antenna BS, and addresses the problems of channel estimation and SE optimization. Both problems have been formulated with the objective of minimizing the MSE. A key aspect is the optimization of the RIS coefficients with spatially correlated channels and EMI. The resulting optimization tasks result in two non-convex problems, both of which are successfully addressed by applying an iterative algorithm based on the principle of alternating optimization, with demonstrated convergence to locally optimal solutions. Numerical results demonstrate the effectiveness of the proposed method and its superiority over state-of-the-art alternatives.

Appendix A

We assume that the receiver has knowledge of the statistics of $\mathbf{x}$ and $\mathbf{w}^{\mathrm{tr}}$ so that the LMMSE estimate of $\mathbf{x}$ can be computed. The spatial correlation matrix $\mathbf{R}_x \in \mathbb{C}^{NM\times NM}$ of $\mathbf{x}$ is

$$\mathbf{R}_x = \mathbb{E}\{\mathbf{x}\mathbf{x}^{\mathrm{H}}\} = \mathbf{R}_{g'_m} \otimes (\mathbf{R}_{g_n} \odot \mathbf{R}_h) = \mathbf{R}_{g'_m} \otimes \mathbf{R}_c, \quad (62)$$

from the statistical independence of $\mathbf{h}$ and $\{\mathbf{g}_n\}$.

Since the interference $\{\mathbf{e}(i); i = 1, 2, \ldots, \tau\}$ is spatially correlated but uncorrelated in time, we have

$$\mathbb{E}\left\{w_{n_1}(i)w_{n_2}(j)^*\right\} = \begin{cases} \sigma_e^2 \mathbf{R}_{g'_m}(n_1, n_2)\boldsymbol{\phi}(i)^{\mathrm{T}}\mathbf{R}_q\boldsymbol{\phi}(i)^* & i = j, \\ 0, & i \neq j, \end{cases} \quad (63)$$

where $\mathbf{R}_{g'_m}(n_1, n_2)$ is the (n_1, n_2)-th element of the correlation matrix $\mathbf{R}_{g'_m}$. Hence, the correlation matrix of $\mathbf{w}^{\mathrm{tr}}$ is given by

$$\mathbf{R}_w^{\mathrm{tr}} = \frac{1}{\sigma_e^2}\mathbb{E}\{\mathbf{w}^{\mathrm{tr}}(\mathbf{w}^{\mathrm{tr}})^{\mathrm{H}}\} = \mathbf{R}_{g'_m} \otimes \left(\left(\boldsymbol{\Phi}_\tau \mathbf{R}_q \boldsymbol{\Phi}_\tau^{\mathrm{H}}\right) \odot \mathbf{I}_\tau\right). \quad (64)$$

The LMMSE estimator is the linear filter designed to minimize the MSE between the channel $\mathbf{x}$ and its estimate $\hat{\mathbf{x}} = \frac{1}{\sqrt{\rho^{\mathrm{tr}}}}\mathbf{R}_x \boldsymbol{\Phi}_{N\tau}^{\mathrm{H}} \left(\mathbf{R}_y^{\mathrm{tr}}\right)^{-1} \mathbf{y}^{\mathrm{tr}}$, i.e.,

$$\mathcal{E}_x(\boldsymbol{\Phi}_\tau) = \mathbb{E}\left\{\|\mathbf{x} - \hat{\mathbf{x}}\|^2\right\} = \mathrm{tr}\left\{\mathbf{R}_x - \mathbf{R}_x \mathbf{Q}^{\mathrm{tr}}(\boldsymbol{\Phi}_\tau)\mathbf{R}_x\right\}. \quad (65)$$

Appendix B
Gradient and Hessian of (52) and (38)

Let $f : \mathbb{C}^{P\times Q} \to \mathbb{R}$ be a function that is twice differentiable, we define the complex *gradient* operator as the PQ-dimensional vector

$$\nabla_{\mathbf{x}} f = \frac{\partial f}{\partial \mathbf{x}^*} \quad (66)$$

where $\mathbf{x} = \mathrm{vec}(\mathbf{X})$. Therefore, if we let $z = (q-1)Q + p$, then it follows that $[\nabla_{\mathbf{x}} f]_z = \frac{\partial f}{\partial \mathbf{x}_z^*} = \frac{\partial f}{\partial \mathbf{X}_{p,q}^*}$.

Considering the fact that $\mathbf{R}_x = \mathbf{R}_{g'_m} \otimes \mathbf{R}_c$, $\mathbf{R}_w^{\mathrm{tr}} = \mathbf{R}_{g'_m} \otimes \left(\left(\boldsymbol{\Phi}_\tau \mathbf{R}_q \boldsymbol{\Phi}_\tau^{\mathrm{H}}\right) \odot \mathbf{I}_\tau\right)$ and $\boldsymbol{\Phi}_{N\tau} = \mathbf{I}_N \otimes \boldsymbol{\Phi}_\tau$, we extract the terms in (52) that are related to $\boldsymbol{\Phi}_\tau$, and represent them sequentially as follows:

$$\mathcal{E}_1^{(k+1)} = \mathrm{tr}\{\boldsymbol{\Lambda}^{(k+1)^{\mathrm{H}}} \boldsymbol{\Lambda}^{(k+1)} \underbrace{\mathbf{R}_{g'_m} \otimes \boldsymbol{\Phi}_\tau \mathbf{R}_c \boldsymbol{\Phi}_\tau^{\mathrm{H}}}_{\mathbf{A}_{\boldsymbol{\Phi}_\tau}}\}, \quad (67)$$

$$\mathcal{E}_2^{(k+1)} = \frac{\sigma_e^2}{\rho^{\mathrm{tr}}}\mathrm{tr}\{\boldsymbol{\Lambda}^{(k+1)^{\mathrm{H}}} \boldsymbol{\Lambda}^{(k+1)} \underbrace{\mathbf{R}_{g'_m} \otimes \left[\left(\boldsymbol{\Phi}_\tau \mathbf{R}_q \boldsymbol{\Phi}_\tau^{\mathrm{H}}\right) \odot \mathbf{I}_\tau\right]}_{\mathbf{B}_{\boldsymbol{\Phi}_\tau}}\}, \quad (68)$$

$$\mathcal{E}_3^{(k+1)} = \mathrm{tr}\{\boldsymbol{\Lambda}^{(k+1)} \underbrace{\mathbf{R}_{g'_m} \otimes \boldsymbol{\Phi}_\tau \mathbf{R}_c}_{\mathbf{C}_{\boldsymbol{\Phi}_\tau}}\}, \quad (69)$$

and

$$\mathcal{E}_4^{(k+1)} = \mathrm{tr}\{\boldsymbol{\Lambda}^{(k+1)^{\mathrm{H}}} \underbrace{\mathbf{R}_{g'_m} \otimes \mathbf{R}_c \boldsymbol{\Phi}_\tau^{\mathrm{H}}}_{\mathbf{D}_{\boldsymbol{\Phi}_\tau}}\}. \quad (70)$$

Applying the chain rule and abbreviating $\mathbf{\Lambda}^{(k+1)}$ to $\mathbf{\Lambda}$, the gradient of (67) to (70) with respect to $[\mathbf{\Phi}_\tau]_{i,m}$ can be expressed as

$$\begin{aligned}\nabla_{[\mathbf{\Phi}_\tau]_{i,m}}\mathcal{E}_1^{(k+1)} &= \mathrm{tr}\left\{\left[\frac{\partial \mathcal{E}_1^{(k+1)}}{\partial \mathbf{A}_{\mathbf{\Phi}_\tau}}\right]^{\mathrm{H}}\frac{\partial \mathbf{A}_{\mathbf{\Phi}_\tau}}{\partial[\mathbf{\Phi}_\tau]_{i,m}}\right\}\\ &= \mathrm{tr}\left\{\mathbf{\Lambda}^{\mathrm{H}}\mathbf{\Lambda}\left[\mathbf{R}_{g'_m}\otimes\frac{(\partial\mathbf{\Phi}_\tau)\mathbf{R}_c\mathbf{\Phi}_\tau^{\mathrm{H}}+\mathbf{\Phi}_\tau\mathbf{R}_c(\partial\mathbf{\Phi}_\tau)^{\mathrm{H}}}{\partial[\mathbf{\Phi}_\tau]_{i,m}}\right]\right\}\\ &= \mathrm{tr}\left\{\mathbf{\Lambda}^{\mathrm{H}}\mathbf{\Lambda}\left[\mathbf{R}_{g'_m}\otimes\left(\mathbf{J}_{i,m}\mathbf{R}_c\mathbf{\Phi}_\tau^{\mathrm{H}}+\mathbf{\Phi}_\tau\mathbf{R}_c\mathbf{J}_{i,m}^{\mathrm{H}}\right)\right]\right\}, \quad (71)\end{aligned}$$

$$\begin{aligned}\nabla_{[\mathbf{\Phi}_\tau]_{i,m}}\mathcal{E}_2^{(k+1)} &= \frac{\sigma_e^2}{\rho^{\mathrm{tr}}}\mathrm{tr}\left\{\left[\frac{\partial \mathcal{E}_2^{(k+1)}}{\partial \mathbf{B}_{\mathbf{\Phi}_\tau}}\right]^{\mathrm{H}}\frac{\partial \mathbf{B}_{\mathbf{\Phi}_\tau}}{\partial[\mathbf{\Phi}_\tau]_{i,m}}\right\} = \frac{\sigma_e^2}{\rho^{\mathrm{tr}}}\cdot\\ &\mathrm{tr}\left\{\mathbf{\Lambda}^{\mathrm{H}}\mathbf{\Lambda}\left[\mathbf{R}_{g'_m}\otimes\left(\frac{(\partial\mathbf{\Phi}_\tau)\mathbf{R}_q\mathbf{\Phi}_\tau^{\mathrm{H}}+\mathbf{\Phi}_\tau\mathbf{R}_q(\partial\mathbf{\Phi}_\tau)^{\mathrm{H}}}{\partial[\mathbf{\Phi}_\tau]_{i,m}}\odot\mathbf{I}_\tau\right)\right]\right\}\\ &= \frac{\sigma_e^2}{\rho^{\mathrm{tr}}}\mathrm{tr}\left\{\mathbf{\Lambda}^{\mathrm{H}}\mathbf{\Lambda}\left[\mathbf{R}_{g'_m}\otimes\left(\left(\mathbf{J}_{i,m}\mathbf{R}_q\mathbf{\Phi}_\tau^{\mathrm{H}}+\mathbf{\Phi}_\tau\mathbf{R}_q\mathbf{J}_{i,m}^{\mathrm{H}}\right)\odot\mathbf{I}_\tau\right)\right]\right\}, \quad (72)\end{aligned}$$

$$\begin{aligned}\nabla_{[\mathbf{\Phi}_\tau]_{i,m}}\mathcal{E}_3^{(k+1)} &= \mathrm{tr}\left\{\left[\frac{\partial \mathcal{E}_3^{(k+1)}}{\partial \mathbf{C}_{\mathbf{\Phi}_\tau}}\right]^{\mathrm{H}}\frac{\partial \mathbf{C}_{\mathbf{\Phi}_\tau}}{\partial[\mathbf{\Phi}_\tau]_{i,m}}\right\}\\ &= \mathrm{tr}\left\{\mathbf{\Lambda}\left(\mathbf{R}_{g'_m}\otimes\frac{(\partial\mathbf{\Phi}_\tau)\mathbf{R}_c}{\partial[\mathbf{\Phi}_\tau]_{i,m}}\right)\right\} = \mathrm{tr}\left\{\mathbf{\Lambda}\left(\mathbf{R}_{g'_m}\otimes\mathbf{J}_{i,m}\mathbf{R}_c\right)\right\}, \quad (73)\end{aligned}$$

and

$$\begin{aligned}\nabla_{[\mathbf{\Phi}_\tau]_{i,m}}\mathcal{E}_4^{(k+1)} &= \mathrm{tr}\left\{\left[\frac{\partial \mathcal{E}_4^{(k+1)}}{\partial \mathbf{D}_{\mathbf{\Phi}_\tau}}\right]^{\mathrm{H}}\frac{\partial \mathbf{D}_{\mathbf{\Phi}_\tau}}{\partial[\mathbf{\Phi}_\tau]_{i,m}}\right\}\\ &= \mathrm{tr}\left\{\mathbf{\Lambda}^{\mathrm{H}}\left(\mathbf{R}_{g'_m}\otimes\frac{\mathbf{R}_c(\partial\mathbf{\Phi}_\tau)^{\mathrm{H}}}{\partial[\mathbf{\Phi}_\tau]_{i,m}}\right)\right\} = \mathrm{tr}\left\{\mathbf{\Lambda}^{\mathrm{H}}\left(\mathbf{R}_{g'_m}\otimes\mathbf{R}_c\mathbf{J}_{i,m}^{\mathrm{H}}\right)\right\}. \quad (74)\end{aligned}$$

Then, letting $z=(m-1)\tau+i$, the z-th element of the gradient of (52) with respect to $\mathbf{\Phi}_\tau$ is computed as

$$\begin{aligned}&[\nabla_{\mathbf{\Phi}_\tau}\mathcal{E}_x(\mathbf{\Lambda},\mathbf{\Phi}_\tau)]_z =\\ &\mathrm{tr}\left\{\mathbf{\Lambda}^{\mathrm{H}}\mathbf{\Lambda}\left[\mathbf{R}_{g'_m}\otimes\left(\mathbf{J}_{i,m}\mathbf{R}_c\mathbf{\Phi}_\tau^{\mathrm{H}}+\mathbf{\Phi}_\tau\mathbf{R}_c\mathbf{J}_{i,m}^{\mathrm{H}}\right)\right]\right\}+\\ &\frac{\sigma_e^2}{\rho^{\mathrm{tr}}}\mathrm{tr}\left\{\mathbf{\Lambda}^{\mathrm{H}}\mathbf{\Lambda}\left[\mathbf{R}_{g'_m}\otimes\left(\left(\mathbf{J}_{i,m}\mathbf{R}_q\mathbf{\Phi}_\tau^{\mathrm{H}}+\mathbf{\Phi}_\tau\mathbf{R}_q\mathbf{J}_{i,m}^{\mathrm{H}}\right)\odot\mathbf{I}_\tau\right)\right]\right\}-\\ &\mathrm{tr}\left\{\mathbf{\Lambda}\left(\mathbf{R}_{g'_m}\otimes\mathbf{J}_{i,m}\mathbf{R}_c\right)\right\}-\mathrm{tr}\left\{\mathbf{\Lambda}^{\mathrm{H}}\left(\mathbf{R}_{g'_m}\otimes\mathbf{R}_c\mathbf{J}_{i,m}^{\mathrm{H}}\right)\right\}, \quad (75)\end{aligned}$$

where $\mathbf{J}_{i,m}$ is a $\tau\times M$ matrix with the (i,m)-th element being 1 and the other elements being 0.

As in the case of the gradient operator, letting $t=(s-1)Q+r$ and $z=(q-1)Q+p$, the complex *Hessian* operator $\nabla^2_{\mathbf{X}}f$ is the $PQ\times PQ$-dimensional Hermitian matrix defined as

$$\left[\nabla^2_{\mathbf{X}}f\right]_{t,z}=\frac{\partial^2 f}{\partial\mathbf{x}_t^*\partial\mathbf{x}_z}=\frac{\partial^2 f}{\partial\mathbf{X}_{r,s}^*\partial\mathbf{X}_{p,q}}. \quad (76)$$

After that, taking derivatives of (71) and (72) with respect to $[\mathbf{\Phi}_\tau]_{i,m}$ again as follows:

$$\begin{aligned}&\frac{\partial\nabla_{[\mathbf{\Phi}_\tau]_{i_1,m_1}}\mathcal{E}_1^{(k+1)}}{\partial[\mathbf{\Phi}_\tau]_{i_2,m_2}}\\ &= \mathrm{tr}\left\{\mathbf{\Lambda}^{\mathrm{H}}\mathbf{\Lambda}\left[\mathbf{R}_{g'_m}\otimes\frac{\mathbf{J}_{i_1,m_1}\mathbf{R}_c(\partial\mathbf{\Phi}_\tau)^{\mathrm{H}}+(\partial\mathbf{\Phi}_\tau)\mathbf{R}_c\mathbf{J}_{i_1,m_1}^{\mathrm{H}}}{\partial[\mathbf{\Phi}_\tau]_{i_2,m_2}}\right]\right\}\\ &= \mathrm{tr}\left\{\mathbf{\Lambda}^{\mathrm{H}}\mathbf{\Lambda}\left[\mathbf{R}_{g'_m}\otimes\left(\mathbf{J}_{i_1,m_1}\mathbf{R}_c\mathbf{J}_{i_2,m_2}^{\mathrm{H}}+\mathbf{J}_{i_2,m_2}\mathbf{R}_c\mathbf{J}_{i_1,m_1}^{\mathrm{H}}\right)\right]\right\}, \quad (77)\end{aligned}$$

and

$$\begin{aligned}&\frac{\partial\nabla_{[\mathbf{\Phi}_\tau]_{i_1,m_1}}\mathcal{E}_2^{(k+1)}}{\partial[\mathbf{\Phi}_\tau]_{i_2,m_2}} = \frac{\sigma_e^2}{\rho^{\mathrm{tr}}}\mathrm{tr}\left\{\mathbf{\Lambda}^{\mathrm{H}}\mathbf{\Lambda}\cdot\right.\\ &\left.\left[\mathbf{R}_{g'_m}\otimes\left(\frac{\mathbf{J}_{i_1,m_1}\mathbf{R}_q(\partial\mathbf{\Phi}_\tau)^{\mathrm{H}}+(\partial\mathbf{\Phi}_\tau)\mathbf{R}_q\mathbf{J}_{i_1,m_1}^{\mathrm{H}}}{\partial[\mathbf{\Phi}_\tau]_{i_2,m_2}}\right)\odot\mathbf{I}_\tau\right]\right\}\\ &= \frac{\sigma_e^2}{\rho^{\mathrm{tr}}}\cdot\\ &\mathrm{tr}\left\{\mathbf{\Lambda}^{\mathrm{H}}\mathbf{\Lambda}\left[\mathbf{R}_{g'_m}\otimes\left(\left(\mathbf{J}_{i_1,m_1}\mathbf{R}_q\mathbf{J}_{i_2,m_2}^{\mathrm{H}}+\mathbf{J}_{i_2,m_2}\mathbf{R}_q\mathbf{J}_{i_1,m_1}^{\mathrm{H}}\right)\odot\mathbf{I}_\tau\right)\right]\right\}, \quad (78)\end{aligned}$$

and introducing $z_1=(m_1-1)\tau+i_1$ and $z_2=(m_2-1)\tau+i_2$, the Hessian of (52) with respect to $\mathbf{\Phi}_\tau$ is computed as.

$$\begin{aligned}&\left[\nabla^2_{\mathbf{\Phi}_\tau}\mathcal{E}_x(\mathbf{\Lambda},\mathbf{\Phi}_\tau)\right]_{z_1,z_2} = \frac{\sigma_e^2}{\rho^{\mathrm{tr}}}\cdot\\ &\mathrm{tr}\left\{\mathbf{\Lambda}^{\mathrm{H}}\mathbf{\Lambda}\left[\mathbf{R}_{g'_m}\otimes\left(\left(\mathbf{J}_{i_1,m_1}\mathbf{R}_q\mathbf{J}_{i_2,m_2}^{\mathrm{H}}+\mathbf{J}_{i_2,m_2}\mathbf{R}_q\mathbf{J}_{i_1,m_1}^{\mathrm{H}}\right)\odot\mathbf{I}_\tau\right)\right]\right\}\\ &+\mathrm{tr}\left\{\mathbf{\Lambda}^{\mathrm{H}}\mathbf{\Lambda}\left[\mathbf{R}_{g'_m}\otimes\left(\mathbf{J}_{i_1,m_1}\mathbf{R}_c\mathbf{J}_{i_2,m_2}^{\mathrm{H}}+\mathbf{J}_{i_2,m_2}\mathbf{R}_c\mathbf{J}_{i_1,m_1}^{\mathrm{H}}\right)\right]\right\}. \quad (79)\end{aligned}$$

Moreover, considering the special scenario of SISO, in this case, $\mathbf{R}_x$ and $\mathbf{R}_w^{\mathrm{tr}}$ degenerate to $\mathbf{R}_c$ and $\left(\left(\mathbf{\Phi}_\tau\mathbf{R}_q\mathbf{\Phi}_\tau^{\mathrm{H}}\right)\odot\mathbf{I}_\tau\right)$. Therefore, the gradient and Hessian of (52) with respect to $\mathbf{\Phi}_\tau$ can be simplified as

$$\begin{aligned}&\nabla_{\mathbf{\Phi}_\tau}\mathcal{E}_x(\mathbf{\Lambda},\mathbf{\Phi}_\tau) =\\ &2\mathbf{\Lambda}^{\mathrm{H}}\mathbf{\Lambda}\mathbf{\Phi}_\tau\mathbf{R}_c+\frac{2\sigma_e^2}{\rho^{\mathrm{tr}}}\left(\left(\mathbf{\Lambda}^{\mathrm{H}}\mathbf{\Lambda}\right)\odot\mathbf{I}_\tau\right)\mathbf{\Phi}_\tau\mathbf{R}_q-2\mathbf{\Lambda}^{\mathrm{H}}\mathbf{R}_c, \quad (80)\end{aligned}$$

and

$$\nabla^2_{\mathbf{\Phi}_\tau}\mathcal{E}_x(\mathbf{\Lambda},\mathbf{\Phi}_\tau)=2\mathbf{\Lambda}^{\mathrm{H}}\mathbf{\Lambda}\otimes\mathbf{R}_c+\frac{2\sigma_e^2}{\rho^{\mathrm{tr}}}\left(\left(\mathbf{\Lambda}^{\mathrm{H}}\mathbf{\Lambda}\right)\odot\mathbf{I}_\tau\right)\otimes\mathbf{R}_q. \quad (81)$$

Similarly, during the data transmission phase, abbreviating $\mathbf{v}^{(k+1)}$ as $\mathbf{v}$, the elements of the gradient and Hessian of (38) with respect to $\boldsymbol{\phi}$ are computed as

$$\begin{aligned}&[\nabla_{\boldsymbol{\phi}}\mathcal{E}_s(\mathbf{v},\boldsymbol{\phi};\hat{\mathbf{x}})]_m = -2\sqrt{\rho}\mathrm{tr}\left\{\hat{\mathbf{x}}\mathbf{v}^{\mathrm{H}}\mathbf{J}_{Nm}\right\}\\ &+\rho\mathrm{tr}\left\{\mathbf{v}\mathbf{v}^{\mathrm{H}}\left[\mathbf{J}_{Nm}\left(\hat{\mathbf{x}}\hat{\mathbf{x}}^{\mathrm{H}}+\mathbf{R}_{\tilde{x}}+\frac{\sigma_e^2}{\rho}\left(\mathbf{R}_{g'_m}\otimes\mathbf{R}_q\right)\right)\mathbf{\Phi}_N^{\mathrm{H}}\right.\right.\\ &\left.\left.+\ \mathbf{\Phi}_N\left(\hat{\mathbf{x}}\hat{\mathbf{x}}^{\mathrm{H}}+\mathbf{R}_{\tilde{x}}+\frac{\sigma_e^2}{\rho}\left(\mathbf{R}_{g'_m}\otimes\mathbf{R}_q\right)\right)\mathbf{J}_{Nm}^{\mathrm{H}}\right]\right\}, \quad (82)\end{aligned}$$

and

$$\begin{aligned}&\left[\nabla^2_{\boldsymbol{\phi}}\mathcal{E}_s(\mathbf{v},\boldsymbol{\phi};\hat{\mathbf{x}})\right]_{m_1,,m_2} =\\ &\rho\mathrm{tr}\left\{\mathbf{v}\mathbf{v}^{\mathrm{H}}\left[\mathbf{J}_{Nm_1}\left(\hat{\mathbf{x}}\hat{\mathbf{x}}^{\mathrm{H}}+\mathbf{R}_{\tilde{x}}+\frac{\sigma_e^2}{\rho}\left(\mathbf{R}_{g'_m}\otimes\mathbf{R}_q\right)\right)\mathbf{J}_{Nm_2}^{\mathrm{H}}\right.\right.\\ &\left.\left.+\ \mathbf{J}_{Nm_2}\left(\hat{\mathbf{x}}\hat{\mathbf{x}}^{\mathrm{H}}+\mathbf{R}_{\tilde{x}}+\frac{\sigma_e^2}{\rho}\left(\mathbf{R}_{g'_m}\otimes\mathbf{R}_q\right)\right)\mathbf{J}_{Nm_1}^{\mathrm{H}}\right]\right\}, \quad (83)\end{aligned}$$

where $\mathbf{J}_{Nm}=\mathbf{I}_N\otimes\mathbf{J}_m$ and $\mathbf{J}_m$ is an M-dimensional vector with the m-th element being 1 and other elements being 0.

Correspondingly, in the SISO scenario, where v degenerates into a complex number, the gradient and Hessian can be written as

$$\nabla_{\boldsymbol{\phi}}\mathcal{E}_s\left(v,\boldsymbol{\phi};\hat{\mathbf{x}}\right) = 2\rho\left|v\right|^2\boldsymbol{\phi}\left(\hat{\mathbf{x}}\hat{\mathbf{x}}^{\mathrm{H}}+\mathbf{R}_{\tilde{x}}+\frac{\sigma_e^2}{\rho}\mathbf{R}_q\right)-2\sqrt{\rho}v^*\hat{\mathbf{x}}^{\mathrm{H}}, \tag{84}$$

and

$$\nabla^2_{\boldsymbol{\phi}}\mathcal{E}_s\left(v,\boldsymbol{\phi};\hat{\mathbf{x}}\right) = 2\rho\left|v\right|^2\left(\hat{\mathbf{x}}\hat{\mathbf{x}}^{\mathrm{H}}+\mathbf{R}_{\tilde{x}}+\frac{\sigma_e^2}{\rho}\mathbf{R}_q\right). \tag{85}$$

ACKNOWLEDGMENT

The authors would like to thank the Editor and the anonymous Reviewers for their careful reading and valuable suggestions that helped to improve the quality of this manuscript.

REFERENCES

[1] C. Liaskos, S. Nie, A. Tsioliaridou, A. Pitsillides, S. Ioannidis, and I. Akyildiz, "A new wireless communication paradigm through software-controlled metasurfaces," *IEEE Commun. Mag.*, vol. 56, no. 9, pp. 162–169, Sept. 2018.

[2] Q. Wu and R. Zhang, "Intelligent reflecting surface enhanced wireless network via joint active and passive beamforming," *IEEE Trans. Wireless Commun.*, vol. 18, no. 11, pp. 5394–5409, Nov. 2019.

[3] M. Di Renzo, A. Zappone, M. Debbah, M.-S. Alouini, C. Yuen, J. de Rosny, and S. Tretyakov, "Smart radio environments empowered by reconfigurable intelligent surfaces: How it works, state of research, and the road ahead," *IEEE J. Sel. Areas Commun.*, vol. 38, no. 11, pp. 2450–2525, Nov. 2020.

[4] E. Björnson, H. Wymeersch, B. Matthiesen, P. Popovski, L. Sanguinetti, and E. de Carvalho, "Reconfigurable intelligent surfaces: A signal processing perspective with wireless applications," *IEEE Signal Process. Mag.*, vol. 39, no. 2, pp. 135–158, Mar. 2022.

[5] Ö. T. Demir and E. Björnson, "Is channel estimation necessary to select phase-shifts for RIS-assisted massive MIMO?" *IEEE Trans. Wireless Commun.*, pp. 1–1, Jun. 2022.

[6] Ö. T. Demir, E. Björnson, and L. Sanguinetti, "Exploiting array geometry for reduced-subspace channel estimation in RIS-aided communications," in *2022 IEEE 12th Sensor Array and Multichannel Signal Processing Workshop (SAM)*, 2022, pp. 455–459.

[7] A. de Jesus Torres, L. Sanguinetti, and E. Björnson, "Electromagnetic interference in RIS-aided communications," *IEEE Wireless Commun. Lett.*, vol. 11, no. 4, pp. 668–672, Apr. 2022.

[8] G. S. Chandra, R. K. Singh, S. Dhok, P. K. Sharma, and P. Kumar, "Downlink URLLC system over spatially correlated RIS channels and electromagnetic interference," *IEEE Wireless Commun. Lett.*, vol. 11, no. 9, pp. 1950–1954, Sep. 2022.

[9] J. David Vega-Sánchez, G. Kaddoum, and F. J. López-Martínez, "Physical layer security of RIS-assisted communications under electromagnetic interference," *IEEE Commun. Lett.*, vol. 26, no. 12, pp. 2870–2874, Dec. 2022.

[10] W.-X. Long, M. Moretti, L. Sanguinetti, and R. Chen, "Channel estimation in RIS-aided communications with interference," *IEEE Wireless Commun. Lett.*, vol. 12, no. 10, pp. 1751–1755, Oct. 2023.

[11] A. Khaleel and E. Basar, "Electromagnetic interference cancellation for RIS-assisted communications," *IEEE Commun. Lett.*, vol. 27, no. 8, pp. 2192–2196, Aug. 2023.

[12] D. Middleton, "Statistical-physical models of electromagnetic interference," *IEEE Trans. Electromagn. Compat.*, vol. EMC-19, no. 3, pp. 106–127, Aug. 1977.

[13] S. Loyka, "Electromagnetic interference in wireless communications: behavioral-level simulation approach," in *2004 IEEE 60th Vehicular Technology Conference*, vol. 6, 2004, pp. 3945–3949.

[14] B. Zheng and R. Zhang, "Intelligent reflecting surface-enhanced OFDM: Channel estimation and reflection optimization," *IEEE Wireless Commun. Lett.*, vol. 9, no. 4, pp. 518–522, Apr. 2020.

[15] Q. Li, M. Wen, E. Basar, G. C. Alexandropoulos, K. J. Kim, and H. V. Poor, "Channel estimation and multipath diversity reception for RIS-empowered broadband wireless systems based on cyclic-prefixed single-carrier transmission," *IEEE Trans. Wireless Commun.*, vol. 22, no. 8, pp. 5145–5156, Aug. 2023.

[16] Z.-Q. He and X. Yuan, "Cascaded channel estimation for large intelligent metasurface assisted massive MIMO," *IEEE Wireless Commun. Lett.*, vol. 9, no. 2, pp. 210–214, Feb. 2020.

[17] J. Mirza and B. Ali, "Channel estimation method and phase shift design for reconfigurable intelligent surface assisted MIMO networks," *IEEE Trans. Cogn. Commun. Netw.*, vol. 7, no. 2, pp. 441–451, Jun. 2021.

[18] L. Wei, C. Huang, G. C. Alexandropoulos, C. Yuen, Z. Zhang, and M. Debbah, "Channel estimation for RIS-empowered multi-user MISO wireless communications," *IEEE Trans. Commun.*, vol. 69, no. 6, pp. 4144–4157, Jun. 2021.

[19] G. Zhou, C. Pan, H. Ren, P. Popovski, and A. L. Swindlehurst, "Channel estimation for RIS-aided multiuser millimeter-wave systems," *IEEE Trans. Signal Process.*, vol. 70, pp. 1478–1492, Mar. 2022.

[20] H. Guo and V. K. N. Lau, "Uplink cascaded channel estimation for intelligent reflecting surface assisted multiuser MISO systems," *IEEE Trans. Signal Process.*, vol. 70, pp. 3964–3977, Jul. 2022.

[21] J. Chen, Y.-C. Liang, H. V. Cheng, and W. Yu, "Channel estimation for reconfigurable intelligent surface aided multi-user mmWave MIMO systems," *IEEE Trans. Wireless Commun.*, vol. 22, no. 10, pp. 6853–6869, Oct. 2023.

[22] Q. Wu and R. Zhang, "Beamforming optimization for wireless network aided by intelligent reflecting surface with discrete phase shifts," *IEEE Trans. Commun.*, vol. 68, no. 3, pp. 1838–1851, Mar. 2020.

[23] K. Feng, Q. Wang, X. Li, and C.-K. Wen, "Deep reinforcement learning based intelligent reflecting surface optimization for MISO communication systems," *IEEE Wireless Commun. Lett.*, vol. 9, no. 5, pp. 745–749, May 2020.

[24] J. Wang, H. Wang, Y. Han, S. Jin, and X. Li, "Joint transmit beamforming and phase shift design for reconfigurable intelligent surface assisted MIMO systems," *IEEE Trans. Cognit. Commun. Netw.*, vol. 7, no. 2, pp. 354–368, Jun. 2021.

[25] K. Zhi, C. Pan, H. Ren, and K. Wang, "Power scaling law analysis and phase shift optimization of RIS-aided massive MIMO systems with statistical CSI," *IEEE Trans. Commun.*, vol. 70, no. 5, pp. 3558–3574, May 2022.

[26] A. Subhash, A. Kammoun, A. Elzanaty, S. Kalyani, Y. H. Al-Badarneh, and M.-S. Alouini, "Optimal phase shift design for fair allocation in RIS-aided uplink network using statistical CSI," *IEEE J. Sel. Areas Commun.*, vol. 41, no. 8, pp. 2461–2475, Aug. 2023.

[27] M. Gao, J. Yang, H. Li, and Y. Wang, "Robust beamforming optimization design for RIS-aided MIMO systems with practical phase shift model and imperfect CSI," *IEEE Internet Things J.*, pp. 1–1, Jun. 2023.

[28] H. Guo and V. K. N. Lau, "Robust deep learning for uplink channel estimation in cellular network under inter-cell interference," *IEEE J. Sel. Areas Commun.*, vol. 41, no. 6, pp. 1873–1887, Jun. 2023.

[29] A. Abrardo, D. Dardari, and M. Di Renzo, "Intelligent reflecting surfaces: Sum-rate optimization based on statistical position information," *IEEE Trans. Wireless Commun.*, vol. 69, no. 10, pp. 7121–7136, Oct. 2021.

[30] F. Jiang, A. Abrardo, K. Keykhoshravi, H. Wymeersch, D. Dardari, and M. D. Renzo, "Two-timescale transmission design and RIS optimization for integrated localization and communications," *IEEE Trans. Wireless Commun.*, vol. 22, no. 12, pp. 8587–8602, Dec. 2023.

[31] E. Björnson and L. Sanguinetti, "Rayleigh fading modeling and channel hardening for reconfigurable intelligent surfaces," *IEEE Wireless Commun. Lett.*, vol. 10, no. 4, pp. 830–834, Apr. 2021.

[32] Ö. T. Demir, E. Björnson, and L. Sanguinetti, "Channel modeling and channel estimation for holographic massive MIMO with planar arrays," *IEEE Wireless Commun. Lett.*, vol. 11, no. 5, pp. 997–1001, May 2022.

[33] D.-S. Shiu, G. Foschini, M. Gans, and J. Kahn, "Fading correlation and its effect on the capacity of multielement antenna systems," *IEEE Trans. Commun.*, vol. 48, no. 3, pp. 502–513, Nov. 2000.

[34] M.-M. Zhao, Q. Wu, M.-J. Zhao, and R. Zhang, "Intelligent reflecting surface enhanced wireless networks: Two-timescale beamforming optimization," *IEEE Trans. Wireless Commun.*, vol. 20, no. 1, pp. 2–17, Jan. 2021.

[35] E. Björnson, J. Hoydis, and L. Sanguinetti, "Massive MIMO networks: Spectral, energy, and hardware efficiency," *Foundations and Trends in Signal Processing*, vol. 11, no. 3-4, pp. 154–655, 2017.

[36] D. Bertsekas, *Nonlinear Programming*, ser. Athena scientific optimization and computation series. Athena Scientific, 2016.

Wen-Xuan Long (Member, IEEE) received her B.S. degree in Rail Transit Signal and Control from Dalian Jiaotong University, Dalian, China, in 2017. She earned her Ph.D. degrees in Information and Communication Engineering from Xidian University, Xi'an, China, and in Information Engineering from the University of Pisa, Pisa, Italy, in 2023. She is currently a postdoctoral research fellow in the Department of Information Engineering at the University of Pisa, Pisa, Italy. Her expertise encompasses wireless communications and signal processing, as well as estimation and detection theory. Her research interests currently focus on high spectral efficiency techniques at the physical layer of B5G/6G wireless communications, including RIS-aided wireless communications and orbital angular momentum (OAM) technology.

Marco Moretti (Member, IEEE) received the degree in electronic engineering from the University of Florence, Florence, Italy, in 1995, and the Ph.D. degree from the Delft University of Technology, Delft, Netherlands, in 2000. From 2000 to 2003, he was a Senior Researcher with Marconi Mobile. He is currently an Associate Professor with the University of Pisa, Pisa, Italy. His research interests include optimization algorithms and artificial intelligence for wireless communications, synchronization, channel estimation, and satellite communications. He is serving as an Area Editor for IEEE TRANSACTIONS ON SIGNAL PROCESSING.

Andrea Abrardo (Senior Member, IEEE) graduated in Electronic Engineering at the University of Florence, Italy, in 1993. From January to November 1994, he worked in the Image Processing and Communications Laboratory of the Department of Electronic Engineering at the University of Florence, collaborating with the Tuscany Region on the development of broadband network infrastructures. From November 1994 to October 1997, he attended the Ph.D. program at the same Department of Electronic Engineering. In 1998, he joined the Department of Information Engineering at the University of Siena, Italy, as a Researcher. His current position is Associate Professor in the Department of Information Engineering at the University of Siena, where he teaches Digital Communications and 5G Technologies. As a result of his research activities, he has published more than 120 works in international journals and conferences. In 2011, he received the Transactions Prize Paper Award from the IEEE Geoscience and Remote Sensing Society. Between 2015 and 2019, he served as Associate Editor (Member of the Editorial Board) of the IEEE Transactions on Wireless Communications (TWCOM) International Journal. During the period from 2017 to 2020, he coordinated, on behalf of the National Inter-University Consortium for Telecommunications (CNIT), the pre-standard 5G trials activity in Milan, collaborating with Vodafone Italia S.p.A. From 2020 to 2024, he was involved in various activities related to European and National projects focused on IoT for industry and transportation, as well as the use of 5G in military applications. His recent research contributions have been directed toward the modeling and optimization of Reconfigurable Intelligent Surfaces (RIS) for communication and sensing applications in beyond 5G and 6G scenarios.

Luca Sanguinetti (S'03-M'07-SM'15) received the Laurea Telecommunications Engineering degree (cum laude) and the Ph.D. degree in information engineering from the University of Pisa, Pisa, Italy, in 2002 and 2005, respectively. From June 2007 to June 2008, he was a Postdoctoral Associate with the Department of Electrical Engineering, Princeton University, Princeton, NJ, USA. From July 2013 to October 2017, he was with the Large Systems and Networks Group, Centrale Supelec, France. He is currently a Full Professor with the Department of Information Engineering, University of Pisa. He has coauthored two textbooks *Massive MIMO Networks*: *Spectral, Energy, and Hardware Efficiency* (2017) and *Foundations of User-Centric Cell-Free Massive MIMO* (2021). His expertise and general interests include wireless communications and signal processing for communications.

Prof. Sanguinetti was the recipient of the 2018 and 2022 Marconi Prize Paper Awards in Wireless Communications and the 2023 Outstanding Paper Award of the IEEE Communications Society, and coauthored a paper that received the Young Best Paper Award from the ComSoc/VTS Italy Section. He was also the recipient of the FP7 Marie Curie IEF 2013, "Dense Deployments for Green Cellular Networks." He was an Associate Editor of the IEEE TRANSACTIONS ON WIRELESS COMMUNICATIONS, IEEE TRANSACTIONS ON COMMUNICATIONS and IEEE SIGNAL PROCESSING LETTERS, the Lead Guest Editor of the IEEE JOURNAL ON SELECTED AREAS OF COMMUNICATIONS Special Issue on Game Theory for Networks, and an Associate Editor of the IEEE JOURNAL ON SELECTED AREAS OF COMMUNICATIONS, series on Green Communications and Networking. He is currently a member of the Executive Editorial Committee of the IEEE TRANSACTIONS ON WIRELESS COMMUNICATIONS.

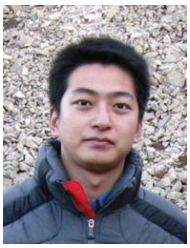

Rui Chen (Member, IEEE) received the B.S., M.S. and Ph.D. degrees in Communications and Information Systems from Xidian University, Xi'an, China, in 2005, 2007 and 2011, respectively. From 2014 to 2015, he was a visiting scholar at Columbia University in the City of New York. He is currently a Full Professor and Ph.D. supervisor in the school of Telecommunications Engineering at Xidian University. He is also the director of Guangzhou Key Laboratory of Multimodal Trafffc Information Perception Processing Technology and Intelligent Equipments. He has published 1 book and over 100 papers in international journals and conferences and held 50 patents. He serves as Associate Editor for International Journal of Electronics, Communications, and Measurement Engineering (IGI Global), Editor for Information Countermeasure Technoloy, Electronics Optics and Control, and comittee members for several conferences. He is a member of IMT-2030 (6G) promotion group. His research interests include broadband wireless communication systems, array signal processing and intelligent transportation systems.